Available online at www.sciencedirect.com
SCIENCE DIRECT®
International Journal of Multiphase Flow 32 (2006) 20–50
International Journal of Multiphase Flow
www.elsevier.com/locate/ijmulflow

Liquid jet in a high Mach number air stream

T. Funada [a], D.D. Joseph [b,*], M. Saitoh [a], S. Yamashita [a]

[a] Department of Digital Engineering, Numazu College of Technology, Ooka 3600, Numazu, Shizuoka 410-8501, Japan
[b] Department of Aerospace Engineering and Mechanics, University of Minnesota, Minneapolis, MN 55455, USA

Received 15 November 2004; received in revised form 24 July 2005

Abstract

The instability of circular liquid jet immersed in a coflowing high velocity air stream is studied assuming that the flow of the viscous gas and liquid is irrotational. The basic velocity profiles are uniform and different. The instabilities are driven by Kelvin–Helmholtz instability due to a velocity difference and neck-down due to capillary instability. Capillary instabilities dominate for large Weber numbers. Kelvin–Helmholtz instability dominates for small Weber numbers. The wavelength for the most unstable wave decreases strongly with the Mach number and attains a very small minimum when the Mach number is somewhat larger than one. The peak growth rates are attained for axisymmetric disturbances ($n = 0$) when the viscosity of the liquid is not too large. The peak growth rates for the first asymmetric mode ($n = 1$) and the associated wavelength are very close to the $n = 0$ mode; the peak growth rate for $n = 1$ modes exceeds $n = 0$ when the viscosity of the liquid jet is large. The effects of viscosity on the irrotational instabilities are very strong. The analysis predicts that breakup fragments of liquids in high speed air streams may be exceedingly small, especially in the transonic range of Mach numbers.

Keywords: Capillary instability; Kelvin–Helmholtz instability; Isentropic compressible gas; Viscous potential flow; Irrotational flow of viscous fluids

* Corresponding author. Tel.: +1 612 626 8000; fax: +1 612 626 1558.
E-mail address: joseph@aem.umn.edu (D.D. Joseph).

0301-9322/$ - see front matter © 2005 Elsevier Ltd. All rights reserved.
doi:10.1016/j.ijmultiphaseflow.2005.07.006

1. Introduction

The problem of an inviscid liquid jet in an inviscid compressible air stream was studied by Chang and Russel (1965), Nayfeh and Saric (1973), Zhou and Lin (1992) and Li and Kelly (1992). Chawla (1975) studied the stability of a sonic gas jet submerged in a liquid. Chang and Russel (1965) and Nayfeh and Saric (1973) consider temporal instability and found that a singularity in the growth rate occurs as the Mach number tends to unity. Chawla (1975) did not find a singular growth rate but he restricted his attention to Mach number one ($M = 1$). Li and Kelly (1992) found that the growth rates reach a sharp maximum when the gas velocity is slightly larger than the one giving $M = 1$ for both axisymmetric and the first non-axisymmetric mode of instability. Lin (2003) cites Li and Kelly (1992) for the growth rate near $M = 1$ in the case of temporal stability.

Here we extend the theory of viscous potential flow of a viscous compressible gas given by Joseph (2003) to the case of perturbations in a compressible gas moving with uniform velocity. We derive a dispersion relation for the perturbations which depend on all the material properties of the incompressible liquid and compressible gas. The effects of shear are neglected, consistent with the assumption that the basic flow can support a discontinuous velocity. We find a sharply peaking growth rate at slightly supersonic value of the gas Mach number under the conditions that Li and Kelly (1992) find steep changes for both axisymmetric and first asymmetric modes. The analysis of Li and Kelly (1992) differs from the one given here in the way that the isentropic flow is represented. They assume that $\mathrm{d}p/\mathrm{d}\rho = c^2$, as in isentropic flow, but they do not account for the usual isentropic relations which tie the density, pressure and velocity together as in our Eq. (4.3).

The first application of viscous potential flow to the problem of capillary instability was done by Funada and Joseph (2002). The problem of combined Kelvin–Helmholtz and capillary instability for an incompressible liquid and gas was done by Funada et al. (2004) who treated also the problem of convective and absolute instability in a comprehensive manner.

The effects of compressibility are very important for transonic and supersonic flow as has already been noted by Lin (2003). These effects include very great increases in growth rates and very sharp decreases in the wavelength for maximum growth. This feature may possibly play a role in the breakup of liquid droplets into fine drops and mist observed in shock tube and wind tunnel experiments (Engel (1958), Joseph et al. (1999, 2002), Theofanous et al. (2003), Varga et al. (2003)).

Chen and Li (1999) did a linear stability analysis for a viscous liquid jet issued into an inviscid moving compressible gas medium. Their analysis differs from ours; they do not assume that motion of the liquid is irrotational; they give results only for the case in which the gas is at rest so that the effects of the basic flow gas velocity is not connected to the basic flow density and pressure as in the case of isotropic flow considered here. They do not compute growth rates for temporal instabilities for supersonic values $M > 1$. Their growth rate curves do not exhibit the same great increases in transonic and supersonic flow found by other authors and here.

The assumption that the gas is inviscid is not justified for jets of liquids into air especially when the air velocity is large. What matters here is the ratios of kinematic viscosities (see Eq. (4.2) in Funada et al. (2004) and Fig. 4 in Funada and Joseph (2001)) and the kinematic viscosity of high speed air in isentropic flow can be much greater than the kinematic viscosity of water.

Experimental results on liquid jets in high speed gas suitable for comparison with this and other analytical studies are not available. The coaxial jet experiments of Varga et al. (2003) discussed in Section 12 is suitable, but they do not present data for transonic and supersonic conditions. Dunne and Cassen (1954, 1956) did some experiments on supersonic liquid jets. They injected high speed jets into air with a spring-loaded injector (1954) and by subjecting the liquid reservoir to a shock wave pressure (1956). These jets are transients and they appear to give rise to Rayleigh–Taylor instabilities on the front face of the jet as in the problem of drop breakup in high speed air and to Kelvin–Helmholtz wave at sides of the jets where the velocity is discontinuous. The data presented by them is not suitable for comparison on the analysis given here.

2. Basic partial differential equations

For isentropic compressible fluids, the equation of continuity, the viscous stress tensor $\mathbf{T}$ and the equation of motion are expressed, in usual notation with the velocity potential ϕ for which $\boldsymbol{v} = \nabla\phi$ and $\nabla \times \boldsymbol{v} = \mathbf{0}$, as

$$\frac{\partial \rho}{\partial t} + \nabla \cdot (\rho \boldsymbol{v}) = 0, \quad \text{hence } \frac{\partial \rho}{\partial t} + (\nabla\phi \cdot \nabla)\rho + \rho\nabla^2\phi = 0, \tag{2.1}$$

$$T_{ij} = \mu\left(\frac{\partial v_i}{\partial x_j} + \frac{\partial v_j}{\partial x_i}\right) - \frac{2\mu}{3}(\nabla \cdot \boldsymbol{v})\delta_{ij} = 2\mu\frac{\partial^2\phi}{\partial x_i \partial x_j} - \frac{2\mu}{3}(\nabla^2\phi)\delta_{ij}, \tag{2.2}$$

$$\frac{\partial \boldsymbol{v}}{\partial t} + (\boldsymbol{v} \cdot \nabla)\boldsymbol{v} = -\frac{1}{\rho}\nabla p + \frac{1}{\rho}\nabla \cdot \mathbf{T} \to \frac{\partial \phi}{\partial t} + \frac{1}{2}|\nabla\phi|^2 + \frac{\gamma}{\gamma - 1}\frac{p}{\rho} - \frac{4}{3}\frac{\mu}{\rho}\nabla^2\phi = B(t). \tag{2.3}$$

The isentropic relation is given by

$$p\rho^{-\gamma} = \text{constant} \equiv A, \quad \text{hence } p = A\rho^{\gamma} \tag{2.4}$$

with the adiabatic exponent γ and the sound velocity c

$$c^2 = \frac{\mathrm{d}p}{\mathrm{d}\rho} = \gamma\frac{p}{\rho}. \tag{2.5}$$

These are used for viscous potential flow (VPF), which reduces to the inviscid potential flow (IPF) when the viscosity vanishes.

3. Cylindrical liquid jet in a compressible gas

A cylindrical liquid jet is surrounded by a compressible gas and is addressed in $0 \leqslant r < a$ (where a is the radius of the cylindrical jet in an undisturbed state) and $-\infty < z < \infty$ in the cylindrical frame (r, θ, z). The equation of continuity, the viscous stress tensor and Bernoulli function are given for the compressible gas

$$\begin{aligned}
&\frac{\partial \rho_{\mathrm{a}}}{\partial t}+(\nabla\phi_{\mathrm{a}}\cdot\nabla)\rho_{\mathrm{a}}+\rho_{\mathrm{a}}\nabla^2\phi_{\mathrm{a}}=0,\\
&T_{ij}^{(a)}=2\mu_{\mathrm{a}}\frac{\partial^2\phi_{\mathrm{a}}}{\partial x_i\partial x_j}-\frac{2\mu_{\mathrm{a}}}{3}(\nabla^2\phi_{\mathrm{a}})\delta_{ij},\\
&\frac{\partial \phi_{\mathrm{a}}}{\partial t}+\frac{1}{2}|\nabla\phi_{\mathrm{a}}|^2+\frac{\gamma}{\gamma-1}\frac{p_{\mathrm{a}}}{\rho_{\mathrm{a}}}-\frac{4}{3}\frac{\mu_{\mathrm{a}}}{\rho_{\mathrm{a}}}\nabla^2\phi_{\mathrm{a}}=B_{\mathrm{a}}(t),\\
&p_{\mathrm{a}}=A\rho_{\mathrm{a}}^{\gamma}\rightarrow\frac{\mathrm{d}p_{\mathrm{a}}}{\mathrm{d}\rho_{\mathrm{a}}}=\gamma A\rho_{\mathrm{a}}^{\gamma-1}=\gamma\frac{p_{\mathrm{a}}}{\rho_{\mathrm{a}}}=c_{\mathrm{a}}^2
\end{aligned}\tag{3.1}$$

and for the liquid

$$\begin{aligned}
&\rho_\ell=\text{constant},\quad \nabla^2\phi_\ell=0,\quad T_{ij}^{(\ell)}=2\mu_\ell\frac{\partial^2\phi_\ell}{\partial x_i\partial x_j},\\
&\frac{\partial \phi_\ell}{\partial t}+\frac{1}{2}|\nabla\phi_\ell|^2+\frac{p_\ell}{\rho_\ell}=B_\ell(t).
\end{aligned}\tag{3.2}$$

Boundary conditions at the interface $r=a+\eta$ (where $\eta=\eta(\theta,z,t)$ is the interface displacement) are the kinematic conditions

$$\frac{\partial\eta}{\partial t}+(\nabla\phi_{\mathrm{a}}\cdot\nabla)\eta=\boldsymbol{n}\cdot\nabla\phi_{\mathrm{a}},\qquad \frac{\partial\eta}{\partial t}+(\nabla\phi_\ell\cdot\nabla)\eta=\boldsymbol{n}\cdot\nabla\phi_\ell \tag{3.3}$$

with the outer normal vector $\boldsymbol{n}$

$$\boldsymbol{n}=\left(1,\frac{-1}{a+\eta}\frac{\partial\eta}{\partial\theta},-\frac{\partial\eta}{\partial z}\right)\Big/\sqrt{1+\left(\frac{1}{a+\eta}\frac{\partial\eta}{\partial\theta}\right)^2+\left(\frac{\partial\eta}{\partial z}\right)^2} \tag{3.4}$$

and the normal stress balance

$$p_\ell-p_{\mathrm{a}}+\left(n_iT_{ij}^{(a)}n_j\right)-\left(n_iT_{ij}^{(\ell)}n_j\right)=\sigma\nabla\cdot\boldsymbol{n}, \tag{3.5}$$

where σ is the interfacial tension coefficient.

4. Basic isentropic relations

A basic state of the gas is with a uniform flow $\bar{\boldsymbol{v}}_{\mathrm{a}}=\nabla\bar{\phi}_{\mathrm{a}}=(0,0,U_{\mathrm{a}})$ in the frame (r,θ,z) and with the constant density $\rho_{\mathrm{a}1}$ and pressure $p_{\mathrm{a}1}$, and a basic state of the liquid is with a uniform flow $\bar{\boldsymbol{v}}_\ell=\nabla\bar{\phi}_\ell=(0,0,U_\ell)$ and with the constant density $\rho_{\ell1}$ and pressure $p_{\ell1}$. The isentropic relation and the Bernoulli function lead for the gas to

$$\begin{aligned}
&p_{\mathrm{a}1}=A\rho_{\mathrm{a}1}^{\gamma}=p_{\mathrm{a}0}\left(\frac{\rho_{\mathrm{a}1}}{\rho_{\mathrm{a}0}}\right)^{\gamma},\qquad \frac{\mathrm{d}p_{\mathrm{a}1}}{\mathrm{d}\rho_{\mathrm{a}0}}=\gamma A\rho_{\mathrm{a}1}^{\gamma-1}=\gamma\frac{p_{\mathrm{a}1}}{\rho_{\mathrm{a}1}}=c_{\mathrm{a}}^2,\\
&\frac{1}{2}U_{\mathrm{a}}^2+\frac{\gamma}{\gamma-1}\frac{p_{\mathrm{a}1}}{\rho_{\mathrm{a}1}}=\frac{1}{2}U_{\mathrm{a}}^2+\frac{c_{\mathrm{a}}^2}{\gamma-1}=\frac{c_{\mathrm{a}0}^2}{\gamma-1}=B_{\mathrm{a}},\quad \text{hence}\quad \left[\frac{\gamma-1}{2}M_{\mathrm{a}}^2+1\right]\frac{\gamma p_{\mathrm{a}1}}{\rho_{\mathrm{a}1}}=\frac{\gamma p_{\mathrm{a}0}}{\rho_{\mathrm{a}0}},
\end{aligned}\tag{4.1}$$

where the Mach number M_a is defined as

$$M_a = \frac{U_a}{c_a} \tag{4.2}$$

and ρ_{a0}, p_{a0} and c_{a0} ($c_{a0}^2 = \gamma p_{a0}/\rho_{a0}$) are defined when $M_a = 0$.

Using (4.1), we have

$$\begin{aligned} &\bar{\rho}_a = \frac{\rho_{a1}}{\rho_{a0}} = \left[\frac{\gamma-1}{2}M_a^2 + 1\right]^{-1/(\gamma-1)}, \qquad \bar{p}_a = \frac{p_{a1}}{p_{a0}} = \left(\frac{\rho_{a1}}{\rho_{a0}}\right)^{\gamma}, \\ &\frac{c_a^2}{c_{a0}^2} = \left[\frac{\gamma-1}{2}M_a^2 + 1\right]^{-1} \quad \text{or } c_a^2 = c_{a0}^2 - \frac{\gamma-1}{2}U_a^2, \end{aligned} \tag{4.3}$$

in which the sound velocity c_a is given as a function of U_a. The thermodynamic properties of the ambient gas depend on the Mach number and the reference state when $M_a = 0$. For air of $\rho_{a0} = 1.2\ \text{kg/m}^3$, $p_{a0} = 1\ \text{atm} = 1.013 \times 10^5\ \text{Pa}$, $c_{a0} = 340\ \text{m/s}$, and $\gamma = 1.4$. When $M_a = 1$, (4.3) gives $c_a^2 = 2c_{a0}^2/(\gamma+1)$ for which $c_a = 310.38\ \text{m/s}$. The third equation in (4.3) shows that $c_a = 0\ \text{m/s}$ when $M_a \to \infty$. Then $U_a^2 = U_{am}^2 = 2c_{a0}^2/(\gamma-1)$ where $U_{am} = 760.26\ \text{m/s}$ is the maximum air velocity.

The Bernoulli function for the liquid leads to

$$\frac{1}{2}U_\ell^2 + \frac{p_{\ell 1}}{\rho_{\ell 1}} = B_\ell. \tag{4.4}$$

The kinematic conditions are satisfied for the unidirectional flows and the interface given by $r = a$. The normal stress balance is given by

$$p_{\ell 1} - p_{a1} = \frac{\sigma}{a}, \tag{4.5}$$

where σ/a denotes the capillary pressure.

5. Linear stability of the cylindrical liquid jet in a compressible gas; dispersion equation

On the basic flows, small disturbances are superimposed as

$$\begin{aligned} &\phi_\ell = U_\ell z + \tilde{\phi}_\ell, \quad \rho_\ell = \rho_{\ell 1}\ (\text{no perturbation}), \quad p_\ell = p_{\ell 1} + \tilde{p}_\ell, \\ &\phi_a = U_a z + \tilde{\phi}_a, \quad \rho_a = \rho_{a1} + \tilde{\rho}_a, \quad p_a = p_{a1} + \tilde{p}_a. \end{aligned} \tag{5.1}$$

The isentropic relation gives

$$p_a = A\rho_a^\gamma, \quad \text{hence} \quad p_{a1} = A\rho_{a1}^\gamma, \quad \tilde{p}_a \approx A\rho_{a1}^\gamma \gamma \frac{\tilde{\rho}_a}{\rho_{a1}} = c_a^2 \tilde{\rho}_a, \tag{5.2}$$

$$\frac{\gamma}{\gamma-1}\frac{p_a}{\rho_a} = \frac{c_a^2}{\gamma-1} + c_a^2\frac{\tilde{\rho}_a}{\rho_{a1}} = \frac{c_a^2}{\gamma-1} + \frac{\tilde{p}_a}{\rho_{a1}}. \tag{5.3}$$

For the gas, we have the equations for the disturbance

$$\left(\frac{\partial}{\partial t} + U_a\frac{\partial}{\partial z}\right)\tilde{\rho}_a + \rho_{a1}\nabla^2\tilde{\phi}_a = 0, \qquad \left(\frac{\partial}{\partial t} + U_a\frac{\partial}{\partial z}\right)\tilde{\phi}_a + c_a^2\frac{\tilde{\rho}_a}{\rho_{a1}} - \frac{4}{3}\frac{\mu_a}{\rho_{a1}}\nabla^2\tilde{\phi}_a = 0, \tag{5.4}$$

hence

$$\left(\frac{\partial}{\partial t}+U_{\mathrm{a}}\frac{\partial}{\partial z}\right)^{2}\tilde{\phi}_{\mathrm{a}}=\left[c_{\mathrm{a}}^{2}+\frac{4}{3}\frac{\mu_{\mathrm{a}}}{\rho_{\mathrm{a1}}}\left(\frac{\partial}{\partial t}+U_{\mathrm{a}}\frac{\partial}{\partial z}\right)\right]\nabla^{2}\tilde{\phi}_{\mathrm{a}}. \tag{5.5}$$

For the liquid, we have the equations for the disturbance

$$\nabla^{2}\tilde{\phi}_{\ell}=0,\qquad \left(\frac{\partial}{\partial t}+U_{\ell}\frac{\partial}{\partial z}\right)\tilde{\phi}_{\ell}+\frac{\tilde{p}_{\ell}}{\rho_{\ell 1}}=0. \tag{5.6}$$

At the interface $r=a+\tilde{\eta}\approx a$ where $\tilde{\eta}\equiv\tilde{\eta}(\theta,z,t)$ is the interface displacement, the kinematic conditions are given by

$$\frac{\partial\tilde{\eta}}{\partial t}+U_{\ell}\frac{\partial\tilde{\eta}}{\partial z}=\frac{\partial\tilde{\phi}_{\ell}}{\partial r},\qquad \frac{\partial\tilde{\eta}}{\partial t}+U_{\mathrm{a}}\frac{\partial\tilde{\eta}}{\partial z}=\frac{\partial\tilde{\phi}_{\mathrm{a}}}{\partial r} \tag{5.7}$$

and the normal stress balance is given, on eliminating the pressures by using the Bernoulli functions, by

$$\begin{aligned}&-\rho_{\mathrm{a1}}\left(\frac{\partial}{\partial t}+U_{\mathrm{a}}\frac{\partial}{\partial z}\right)\tilde{\phi}_{\mathrm{a}}+2\mu_{\mathrm{a}}\left[\nabla^{2}\tilde{\phi}_{\mathrm{a}}-\frac{\partial^{2}\tilde{\phi}_{\mathrm{a}}}{\partial r^{2}}\right]+\rho_{\ell 1}\left(\frac{\partial}{\partial t}+U_{\ell}\frac{\partial}{\partial z}\right)\tilde{\phi}_{\ell}+2\mu_{\ell}\frac{\partial^{2}\tilde{\phi}_{\ell}}{\partial r^{2}}\\&\quad=\sigma\left(\frac{\partial^{2}\tilde{\eta}}{\partial z^{2}}+\frac{1}{a^{2}}\frac{\partial^{2}\tilde{\eta}}{\partial\theta^{2}}+\frac{\tilde{\eta}}{a^{2}}\right).\end{aligned} \tag{5.8}$$

The solution to the stability problem above formulated is expressed by normal modes

$$\begin{aligned}&\tilde{\phi}_{\ell}=-\mathrm{i}\frac{\omega-kU_{\ell}}{kI_{n}'(ka)}HI_{n}(kr)E+\mathrm{c.c.},\qquad \tilde{\phi}_{\mathrm{a}}=-\mathrm{i}\frac{\omega-kU_{\mathrm{a}}}{\kappa K_{n}'(\kappa a)}HK_{n}(\kappa r)E+\mathrm{c.c.},\\&\tilde{\eta}=HE+\mathrm{c.c.},\end{aligned} \tag{5.9}$$

where $E\equiv\exp(\mathrm{i}kz+\mathrm{i}n\theta-\mathrm{i}\omega t)$ with the complex angular frequency $\omega=\omega_{\mathrm{R}}+\mathrm{i}\omega_{\mathrm{I}}$ and the real wave number k, n denotes the azimuthal mode. $I_n(kr)$ and $K_n(\kappa r)$ are the modified Bessel functions, where the prime denotes the derivative $I_n'(ka)=\mathrm{d}I_n(ka)/\mathrm{d}(ka)$. The Bessel functions satisfy the equations

$$\begin{aligned}&\nabla^{2}\tilde{\phi}_{\ell}=\frac{\partial^{2}\tilde{\phi}_{\ell}}{\partial r^{2}}+\frac{1}{r}\frac{\partial\tilde{\phi}_{\ell}}{\partial r}+\frac{1}{r^{2}}\frac{\partial^{2}\tilde{\phi}_{\ell}}{\partial\theta^{2}}+\frac{\partial^{2}\tilde{\phi}_{\ell}}{\partial z^{2}}=\frac{\partial^{2}\tilde{\phi}_{\ell}}{\partial r^{2}}+\frac{1}{r}\frac{\partial\tilde{\phi}_{\ell}}{\partial r}-\frac{n^{2}}{r^{2}}\tilde{\phi}_{\ell}-k^{2}\tilde{\phi}_{\ell}=0,\\&\nabla^{2}\tilde{\phi}_{\mathrm{a}}-(\kappa^{2}-k^{2})\tilde{\phi}_{\mathrm{a}}=\frac{\partial^{2}\tilde{\phi}_{\mathrm{a}}}{\partial r^{2}}+\frac{1}{r}\frac{\partial\tilde{\phi}_{\mathrm{a}}}{\partial r}-\frac{n^{2}}{r^{2}}\tilde{\phi}_{\mathrm{a}}-\kappa^{2}\tilde{\phi}_{\mathrm{a}}=0,\end{aligned} \tag{5.10}$$

with

$$\kappa=\sqrt{k^{2}-\frac{(\omega-kU_{\mathrm{a}})^{2}}{c_{\mathrm{a}}^{2}-\frac{4\mathrm{i}\mu_{\mathrm{a}}}{3\rho_{\mathrm{a1}}}(\omega-kU_{\mathrm{a}})}}, \tag{5.11}$$

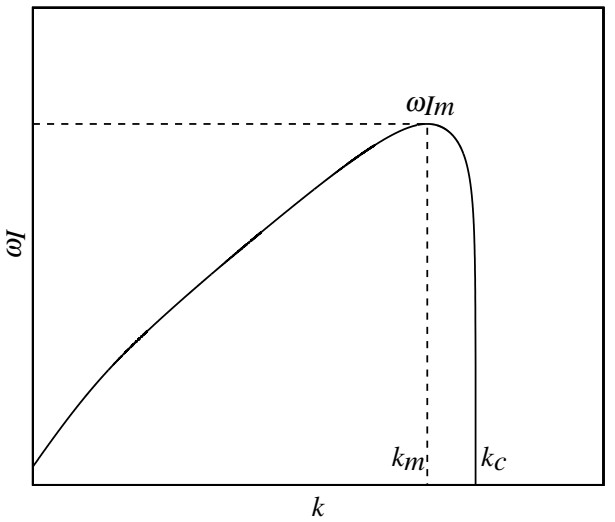

Fig. 1. The form of a typical graph of the growth rate ω_{I} versus k. ω_{Im} is the maximum growth, $\lambda_{\mathrm{m}} = 2\pi/k_{\mathrm{m}}$ is the wavelength of the fastest growing wave. k_{c} is the cut-off wave number. ω_{Im} and k_{m} are called peak values.

which arise from (5.5) and (5.6). Substituting (5.9) into (5.7) and (5.8), we find the dispersion relation

$$[\rho_{\mathrm{a}1}(\omega - kU_{\mathrm{a}})^2 - 2\mathrm{i}\mu_{\mathrm{a}}(\kappa^2 - k^2)(\omega - kU_{\mathrm{a}})]\frac{kK_n(\kappa a)}{\kappa K_n'(\kappa a)} - \rho_{\ell 1}(\omega - kU_{\ell})^2\frac{I_n(ka)}{I_n'(ka)}$$
$$+ 2\mathrm{i}\mu_{\mathrm{a}}k\kappa(\omega - kU_{\mathrm{a}})\frac{K_n''(\kappa a)}{K_n'(\kappa a)} - 2\mathrm{i}\mu_{\ell}k^2(\omega - kU_{\ell})\frac{I_n''(ka)}{I_n'(ka)} + \sigma\left(k^2 - \frac{1-n^2}{a^2}\right)k = 0. \tag{5.12}$$

The wave number k_{m} and maximum growth rate ω_{Im} given by $\omega_{\mathrm{Im}} = \max\omega_{\mathrm{I}}(k) = \omega_{\mathrm{I}}(k_{\mathrm{m}})$ define the disturbance which is expected to appear in experiments. A typical dispersion relation is shown in Fig. 1. The cut-off wave number is the border of instability $\omega_{\mathrm{I}}(k_{\mathrm{c}}) = 0$.

6. Stability problem in dimensionless form

The scaling is made as

$$[\text{length}, \text{velocity}, \text{time}] = [d, c_{\mathrm{a}}, d/c_{\mathrm{a}}], \tag{6.1}$$

Table 1
Properties of air–water

Diameter of liquid jet d	0.001 m
Air viscosity μ_{a}	1.8×10^{-5} N s/m^2
Air density $\rho_{\mathrm{a}0}$	1.2 kg/m^3
Water density $\rho_{\ell 1}$	1000 kg/m^3
Surface tension coefficient σ	0.075 N/m
Ratio of the specific heats γ (air)	1.4

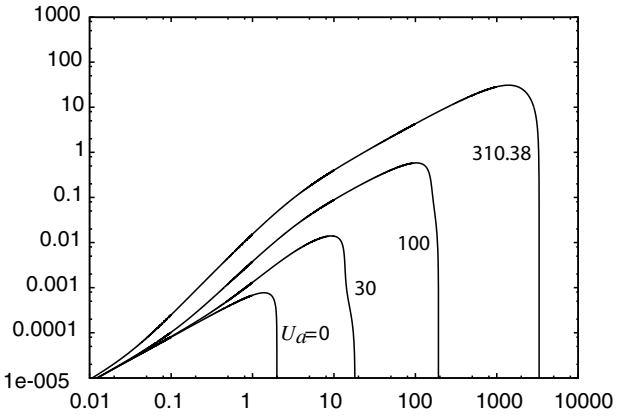

Fig. 2. The growth rate ω_I versus k in the axisymmetric $n = 0$ mode for IPF, using the material parameters (Table 1) for stationary water and air with $U_a = 0$, 30, 100 and 310.38 m/s. The values can be converted into dimensionless form (M, W) using Table 2.

Table 2
Typical values and non-dimensional parameters for various U_a ($U_\ell = 0$)

U_a, m/s	c_a	p_{a1}	ρ_{a1}	ℓ	M	R	W
0.00	3.400e+02	1.013e+05	1.200e+0	1.200e−03	0.000e+0	3.400e+05	6.488e−07
0.10	3.400e+02	1.013e+05	1.200e+0	1.200e−03	2.941e−04	3.400e+05	6.488e−07
0.20	3.400e+02	1.013e+05	1.200e+0	1.200e−03	5.882e−04	3.400e+05	6.488e−07
0.50	3.400e+02	1.013e+05	1.200e+0	1.200e−03	1.471e−03	3.400e+05	6.488e−07
1.00	3.400e+02	1.013e+05	1.200e+0	1.200e−03	2.941e−03	3.400e+05	6.488e−07
5.00	3.400e+02	1.013e+05	1.200e+0	1.200e−03	1.471e−02	3.400e+05	6.488e−07
10.00	3.400e+02	1.012e+05	1.199e+0	1.199e−03	2.941e−02	3.400e+05	6.489e−07
20.00	3.399e+02	1.011e+05	1.198e+0	1.198e−03	5.884e−02	3.399e+05	6.492e−07
50.00	3.393e+02	9.977e+04	1.187e+0	1.187e−03	1.474e−01	3.393e+05	6.516e−07
70.00	3.386e+02	9.833e+04	1.175e+0	1.175e−03	2.068e−01	3.386e+05	6.543e−07
100.00	3.370e+02	9.530e+04	1.149e+0	1.149e−03	2.967e−01	3.370e+05	6.602e−07
150.00	3.333e+02	8.816e+04	1.087e+0	1.087e−03	4.500e−01	3.333e+05	6.751e−07
200.00	3.280e+02	7.881e+04	1.003e+0	1.003e−03	6.097e−01	3.280e+05	6.970e−07
250.00	3.211e+02	6.787e+04	9.014e−01	9.014e−04	7.786e−01	3.211e+05	7.274e−07
300.00	3.124e+02	5.602e+04	7.860e−01	7.860e−04	9.603e−01	3.124e+05	7.684e−07
310.38	3.104e+02	5.351e+04	7.607e−01	7.607e−04	1.000e+00	3.104e+05	7.786e−07
350.00	3.018e+02	4.401e+04	6.616e−01	6.616e−04	1.160e+00	3.018e+05	8.233e−07
400.00	2.891e+02	3.258e+04	5.337e−01	5.337e−04	1.383e+00	2.891e+05	8.971e−07
450.00	2.740e+02	2.239e+04	4.082e−01	4.082e−04	1.642e+00	2.740e+05	9.987e−07
500.00	2.561e+02	1.395e+04	2.911e−01	2.911e−04	1.952e+00	2.561e+05	1.143e−06
550.00	2.347e+02	7.573e+03	1.882e−01	1.882e−04	2.343e+00	2.347e+05	1.361e−06
600.00	2.088e+02	3.338e+03	1.048e−01	1.048e−04	2.873e+00	2.088e+05	1.720e−06
650.00	1.764e+02	1.023e+03	4.505e−02	4.505e−05	3.686e+00	1.764e+05	2.412e−06
700.00	1.327e+02	1.395e+02	1.085e−02	1.085e−05	5.276e+00	1.327e+05	4.261e−06
750.00	5.568e+01	3.199e−01	1.413e−04	1.413e−07	1.347e+01	5.568e+04	2.419e−05
760.00	8.944e+00	8.832e−07	1.512e−08	1.512e−11	8.497e+01	8.944e+03	9.375e−04
760.20	4.381e+00	5.973e−09	4.262e−10	4.262e−13	1.735e+02	4.381e+03	3.908e−03

Table 3
The table of peak values for $\mu_\ell = 1$ cP in compressible gas

U_a	$\mu_\ell = 1$ cP		$n = 0$			$n = 1$		
	R	v	ω_{Im}	k_m	k_c	ω_{Im}	k_m	k_c
0.00	3.400e+05	1.500e+01	7.790e−04	1.387e+00	1.999e+00	–	–	–
0.50	3.400e+05	1.500e+01	7.797e−04	1.396e+00	1.999e+00	1.228e−07	1.027e−02	2.341e−01
10.00	3.400e+05	1.501e+01	1.140e−03	1.891e+00	3.583e+00	2.218e−05	1.666e−01	2.962e+00
100.00	3.370e+05	1.567e+01	5.905e−01	1.027e+02	1.999e+02	5.902e−01	1.027e+02	1.999e+02
310.38	3.104e+05	2.366e+01	3.033e+01	1.432e+03	3.790e+03	3.033e+01	1.432e+03	3.790e+03
500.00	2.561e+05	6.183e+01	6.707e+00	9.919e+02	2.359e+03	6.707e+00	9.919e+02	2.359e+03
600.00	2.088e+05	1.717e+02	2.950e+00	8.317e+02	1.837e+03	2.950e+00	8.317e+02	1.837e+03
700.00	1.327e+05	1.658e+03	3.401e+00	1.153e+03	2.062e+03	3.401e+00	1.153e+03	2.062e+03
750.00	5.568e+04	1.274e+05	1.038e+01	1.315e+03	2.350e+03	1.038e+01	1.315e+03	2.350e+03
760.20	4.381e+03	4.224e+10	1.391e+02	1.351e+03	2.413e+03	1.391e+02	1.351e+03	2.413e+03

Table 4
The table of peak values for $\mu_\ell = 300$ cP in compressible gas

U_a	$\mu_\ell = 300$ cP		$n = 0$			$n = 1$		
	R	v	ω_{Im}	k_m	k_c	ω_{Im}	k_m	k_c
0.00	1.133e+03	5.000e−02	3.711e−04	9.325e−01	1.999e+00	–	–	–
0.50	1.133e+03	5.000e−02	3.713e−04	9.325e−01	1.999e+00	5.698e−08	1.000e−02	1.360e−02
10.00	1.133e+03	5.002e−02	4.635e−04	1.207e+00	2.683e+00	1.735e−05	5.815e−02	1.801e−01
100.00	1.123e+03	5.223e−02	4.801e−02	2.026e+01	1.585e+02	4.755e−02	2.089e+01	1.585e+02
310.38	1.035e+03	7.887e−02	1.515e+00	1.657e+02	1.522e+03	1.515e+00	1.657e+02	1.522e+03
500.00	8.537e+02	2.061e−01	9.396e−02	1.144e+01	4.645e+01	9.367e−02	1.126e+01	4.645e+01
600.00	6.960e+02	5.723e−01	3.802e−02	6.985e+00	2.341e+01	3.809e−02	6.391e+00	2.323e+01
700.00	4.422e+02	5.528e+00	4.186e−03	2.638e+00	6.148e+00	7.160e−03	1.252e+00	5.473e+00
750.00	1.856e+02	4.246e+02	2.437e−03	1.027e+00	2.233e+00	2.471e−03	3.916e−01	1.135e+00
760.20	1.460e+01	1.408e+08	2.910e−02	9.496e−01	2.053e+00	3.356e−02	3.970e−01	1.135e+00

Table 5
The table of peak values for $\mu_\ell = 800$ cP in compressible gas

U_a	$\mu_\ell = 800$ cP		$n = 0$			$n = 1$		
	R	v	ω_{Im}	k_m	k_c	ω_{Im}	k_m	k_c
0.00	4.250e+02	1.875e−02	2.006e−04	6.769e−01	1.999e+00	–	–	–
0.50	4.250e+02	1.875e−02	2.006e−04	6.778e−01	1.999e+00	–	–	–
10.00	4.250e+02	1.876e−02	2.324e−04	8.884e−01	2.683e+00	1.490e−05	3.943e−02	1.108e−01
100.00	4.213e+02	1.959e−02	1.972e−02	1.216e+01	1.585e+02	1.929e−02	1.360e+01	1.585e+02
310.38	3.880e+02	2.958e−02	7.069e−01	1.135e+02	1.522e+03	7.072e−01	1.144e+02	1.522e+03
500.00	3.202e+02	7.729e−02	3.912e−02	5.365e+00	2.845e+01	4.268e−02	3.997e+00	2.836e+01
600.00	2.610e+02	2.146e−01	1.451e−02	3.592e+00	1.432e+01	2.093e−02	1.747e+00	1.414e+01
700.00	1.658e+02	2.073e+00	1.264e−03	1.396e+00	4.402e+00	5.576e−03	5.752e−01	3.430e+00
750.00	6.960e+01	1.592e+02	1.277e−03	7.309e−01	2.179e+00	1.945e−03	2.251e−01	6.688e−01
760.20	5.476e+00	5.280e+07	1.561e−02	6.805e−01	2.008e+00	2.644e−02	2.368e−01	6.832e−01

with $d = 2a$. The dimensionless variables are

$$(\hat{r}, \theta, \hat{z}) = \left(\frac{r}{d}, \theta, \frac{z}{d}\right), \qquad \hat{t} = \frac{c_a}{d} t. \tag{6.2}$$

Table 6
The table of peak values for $\mu_\ell = 8000$ cP in compressible gas

U_a	$\mu_\ell = 8000$ cP		$n = 0$			$n = 1$		
	R	v	ω_{Im}	k_m	k_c	ω_{Im}	k_m	k_c
0.00	4.250e+01	1.875e−03	2.656e−05	2.431e−01	1.999e+00	–	–	–
0.50	4.250e+01	1.875e−03	2.656e−05	2.431e−01	1.999e+00	–	–	–
10.00	4.250e+01	1.876e−03	2.762e−05	4.177e−01	2.683e+00	8.636e−06	1.252e−02	3.556e−02
100.00	4.213e+01	1.959e−03	2.069e−03	8.065e+00	1.585e+02	2.219e−03	8.326e−01	1.585e+02
310.38	3.880e+01	2.958e−03	1.096e−01	5.104e+01	1.513e+03	1.094e−01	5.338e+01	1.513e+03
500.00	3.202e+01	7.729e−03	2.469e−03	1.828e+00	2.143e+01	1.646e−02	8.902e−01	1.981e+01
600.00	2.610e+01	2.146e−02	6.813e−04	1.387e+00	1.333e+01	9.624e−03	5.635e−01	1.234e+01
700.00	1.658e+01	2.073e−01	1.026e−04	6.481e−01	3.817e+00	2.388e−03	2.584e−01	2.386e+00
750.00	6.960e+00	1.592e+01	1.635e−04	2.692e−01	2.170e+00	1.025e−03	5.671e−02	1.990e−01
760.20	5.476e−01	5.280e+06	2.061e−03	2.431e−01	1.999e+00	1.348e−02	5.977e−02	2.161e−01

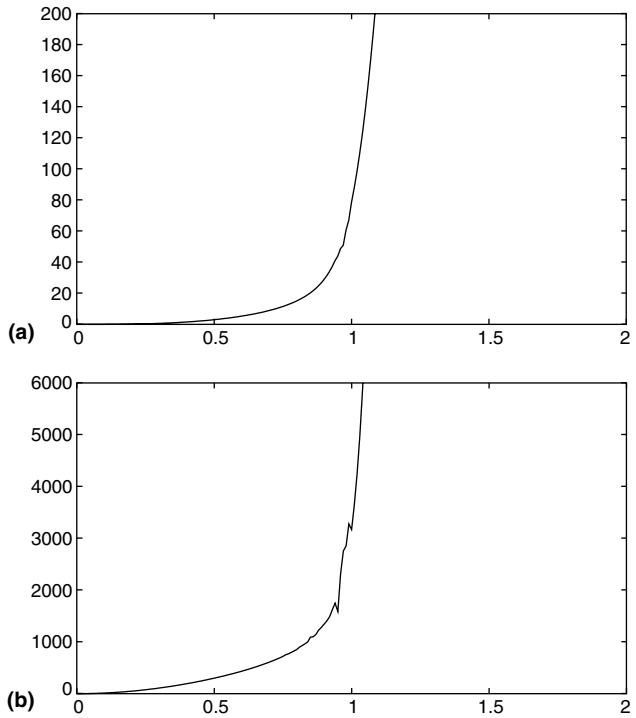

Fig. 3. (a) The maximum growth rate ω_{Im} versus M and (b) k_m versus M for IPF of $n = 0$ in compressible gas.

The hat on the independent variables are omitted for brevity. Then we may scale as

$$\frac{\phi_\ell}{c_a d} = \frac{U_\ell}{c_a}\hat{z} + \frac{\tilde{\phi}_\ell}{c_a d} = M_\ell \hat{z} + \hat{\phi}_\ell, \quad \frac{\rho_\ell}{\rho_{\ell 1}} = 1, \quad \frac{p_\ell}{\rho_{\ell 1} c_a^2} = \bar{p}_{\ell 1} + \frac{\tilde{p}_\ell}{\rho_{\ell 1} c_a^2} = \bar{p}_{\ell 1} + \hat{p}_\ell,$$
$$\frac{\phi_a}{c_a d} = \frac{U_a}{c_a}\hat{z} + \frac{\tilde{\phi}_a}{c_a d} = M_a \hat{z} + \hat{\phi}_a, \qquad \frac{\rho_a}{\rho_{a1}} = \frac{\rho_{a1}}{\rho_{a1}} + \frac{\tilde{\rho}_a}{\rho_{a1}} = 1 + \hat{\rho}_a, \quad \hat{p}_a = \frac{\tilde{p}_a}{\rho_{\ell 1} c_a^2} = \frac{\tilde{\rho}_a}{\rho_{\ell 1}} = \ell \hat{\rho}_a, \tag{6.3}$$

where $\bar{}$ denotes the normalized basic flow and $\hat{}$ denotes the normalized disturbances, and the parameters are defined as

$$\ell = \frac{\rho_{a1}}{\rho_{\ell 1}}, \quad m = \frac{\mu_a}{\mu_\ell}, \quad v = \frac{\mu_a}{\mu_\ell}\frac{\rho_{\ell 1}}{\rho_{a1}} = \frac{m}{\ell}, \quad M_\ell = \frac{U_\ell}{c_a}, \quad M_a = \frac{U_a}{c_a},$$
$$R = \frac{\rho_{\ell 1} c_a d}{\mu_\ell}, \quad W = \frac{\sigma}{\rho_{\ell 1} d c_a^2}, \tag{6.4}$$

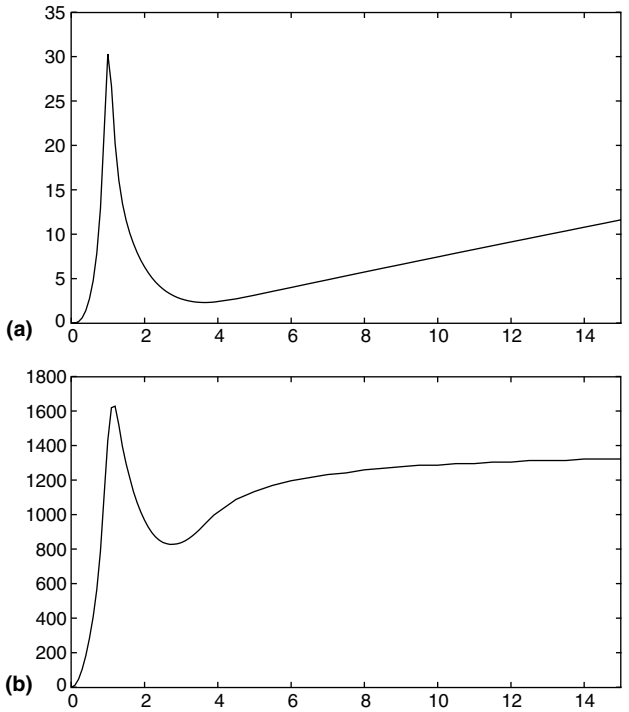

Fig. 4. (a) The maximum growth rate ω_{Im} versus M and (b) k_m versus M for VPF ($\mu_\ell = 1$ cP) of $n = 0$ in compressible gas.

where the basic state of the gas is the function of the Mach number, with

$$\begin{aligned}
&\frac{\rho_{a1}}{\rho_{a0}} = Q(M_a)^{-1/(\gamma-1)}, \quad \text{where } Q(M_a) \equiv \frac{\gamma-1}{2}M_a^2 + 1,\\
&\ell = \ell_0 Q(M_a)^{-1/(\gamma-1)}, \quad \ell_0 = \rho_{a0}/\rho_{\ell 1}, \quad \frac{p_{a1}}{p_{a0}} = \left(\frac{\rho_{a1}}{\rho_{a0}}\right)^{\gamma}, \quad \frac{c_a^2}{c_{a0}^2} = \frac{1}{Q(M_a)},\\
&R = R_0/Q(M_a), \quad R_0 = \frac{\rho_{\ell 1} c_{a0} d}{\mu_\ell}, \qquad W = W_0 Q(M_a), \quad W_0 = \frac{\sigma}{\rho_{\ell 1} d c_{a0}^2},\\
&\frac{1}{2}M_\ell^2 + \bar{p}_{\ell 1} = \text{constant}.
\end{aligned} \tag{6.5}$$

For the gas,

$$\left(\frac{\partial}{\partial t} + M_a\frac{\partial}{\partial z}\right)\hat{\rho}_a + \nabla^2\hat{\phi}_a = 0, \qquad \ell\left(\frac{\partial}{\partial t} + M_a\frac{\partial}{\partial z}\right)\hat{\phi}_a + \hat{p}_a - \frac{4m}{3R}\nabla^2\hat{\phi}_a = 0. \tag{6.6}$$

The combination leads to

$$\left(\frac{\partial}{\partial t} + M_a\frac{\partial}{\partial z}\right)^2\hat{\phi}_a = \left[1 + \frac{4m}{3\ell R}\left(\frac{\partial}{\partial t} + M_a\frac{\partial}{\partial z}\right)\right]\nabla^2\hat{\phi}_a. \tag{6.7}$$

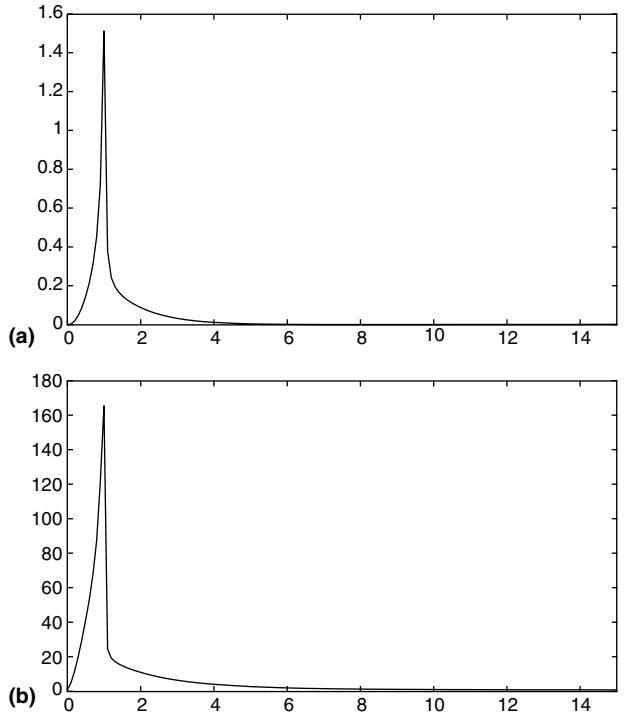

Fig. 5. (a) The maximum growth rate ω_{Im} versus M and (b) k_m versus M for VPF ($\mu_\ell = 300$ cP) of $n = 0$ in compressible gas.

For the liquid,

$$\nabla^2\hat{\phi}_\ell = 0, \quad \left(\frac{\partial}{\partial t} + M_\ell \frac{\partial}{\partial z}\right)\hat{\phi}_\ell + \hat{p}_\ell = 0. \tag{6.8}$$

At the interface $r = 1/2 + \hat{\eta} \approx 1/2$ where $\hat{\eta} \equiv \hat{\eta}(\theta, z, t)$ is the interface displacement, the kinematic conditions are given by

$$\frac{\partial\hat{\eta}}{\partial t} + M_\ell \frac{\partial\hat{\eta}}{\partial z} = \frac{\partial\hat{\phi}_\ell}{\partial r}, \qquad \frac{\partial\hat{\eta}}{\partial t} + M_\mathrm{a} \frac{\partial\hat{\eta}}{\partial z} = \frac{\partial\hat{\phi}_\mathrm{a}}{\partial r} \tag{6.9}$$

and the normal stress balance is given by

$$-\ell\left(\frac{\partial}{\partial t} + M_\mathrm{a}\frac{\partial}{\partial z}\right)\hat{\phi}_\mathrm{a} + \frac{2m}{R}\left(\nabla^2\hat{\phi}_\mathrm{a} - \frac{\partial^2\hat{\phi}_\mathrm{a}}{\partial r^2}\right) + \left(\frac{\partial}{\partial t} + M_\ell\frac{\partial}{\partial z}\right)\hat{\phi}_\ell + \frac{2}{R}\frac{\partial^2\hat{\phi}_\ell}{\partial r^2} = W\left(\frac{\partial^2\hat{\eta}}{\partial z^2} + \frac{\partial^2\hat{\eta}}{\partial\theta^2} + \hat{\eta}\right). \tag{6.10}$$

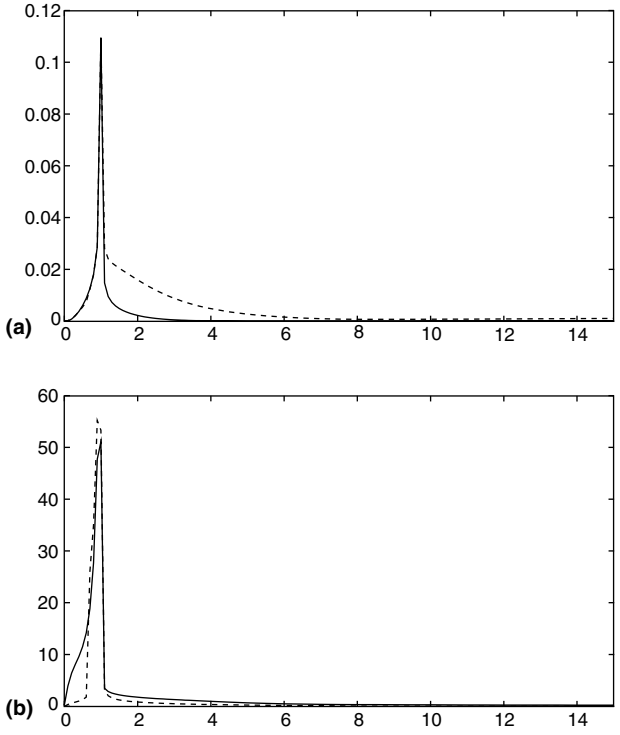

Fig. 6. (a) The maximum growth rate ω_Im versus M and (b) k_m versus M. VPF ($\mu_\ell = 8000$ cP); $n = 0$ in compressible gas (solid line) and $n = 1$ in compressible gas (dashed line).

The solution to the stability problem above formulated is expressed as

$$\hat{\phi}_\ell = -\mathrm{i}\frac{\omega - kM_\ell}{kI_n'(k/2)}\hat{H}I_n(kr)E + \text{c.c.}, \qquad \hat{\phi}_\mathrm{a} = -\mathrm{i}\frac{\omega - kM_\mathrm{a}}{\kappa K_n'(\kappa/2)}\hat{H}K_n(\kappa r)E + \text{c.c.},$$
$$\hat{\eta} = \hat{H}E + \text{c.c.}, \tag{6.11}$$

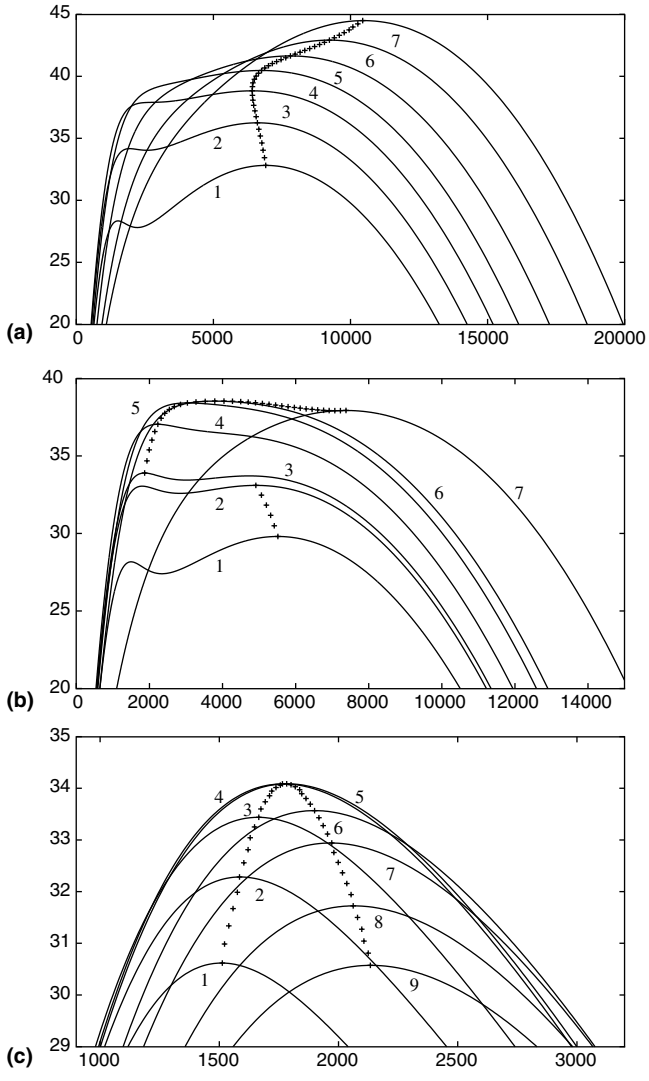

Fig. 7. Growth rate versus wave number for stationary liquid jet ($U_\ell = 0$) in transonic air. $U_\mathrm{a} = [1,2,3,4,5,6,7] = [290.08, 302.08, 314.08, 326.08, 340.08, 356.08, 370.08]$ m/s. (a) $\mu_\ell = 0.15$ cP: as U_a increases, the maximum growth rate marked by + increases monotonically without limit, (b) $\mu_\ell = 0.175$ cP: as U_a increases, the maximum growth rate marked by + increases, changes to another peak, attains the maximum near $U_\mathrm{a} = 310.38$ m/s ($M = 1$), and then decreases and (c) $\mu_\ell = 0.5$ cP: as U_a increases, the maximum growth rate marked by + increases, attains the maximum near $U_\mathrm{a} = 310.38$ m/s ($M = 1$), and then decreases.

where $E \equiv \exp(\mathrm{i}kz + \mathrm{i}n\theta - \mathrm{i}\omega t)$ with the complex angular frequency $\omega = \omega_{\mathrm{R}} + \mathrm{i}\omega_{\mathrm{I}}$ and the real wave number k, $I_n(kr)$ and $K_n(\kappa r)$ are the modified Bessel functions, the prime denotes the derivative: $I_n'(k/2) = \mathrm{d}I_n(k/2)/\mathrm{d}(k/2)$, and κ is defined as

$$\kappa = \sqrt{k^2 - \frac{\theta^2}{1 - \frac{4\mathrm{i}m}{\ell R}\theta}}, \tag{6.12}$$

Table 7
Table of peak values of $n = 0$ and $n = 1$ for various M, IPF in compressible gas

M	$n = 0$			$n = 1$		
	ω_{Im}	k_{m}	k_{c}	ω_{Im}	k_{m}	k_{c}
0.00	7.821e−04	1.396e+00	2.008e+00	–	–	–
0.50	3.000e+00	2.989e+02	4.483e+02	3.000e+00	2.989e+02	4.483e+02
0.75	1.149e+01	7.192e+02	1.081e+03	1.149e+01	7.147e+02	1.081e+03
1.00	7.853e+01	3.169e+03	4.933e+03	7.853e+01	3.169e+03	4.933e+03
1.10	2.302e+02	1.540e+04	2.107e+04	2.302e+02	1.540e+04	2.107e+04
1.50	1.120e+03	2.656e+05	2.755e+05	1.120e+03	2.656e+05	2.755e+05
2.00	1.576e+03	8.560e+05	8.632e+05	1.576e+03	8.560e+05	8.632e+05

Table 8
Table of peak values for various M (VPF: $\mu_\ell = 1$ cP, $m = 1.8 \times 10^{-2}$)

M	$n = 0$			$n = 1$		
	ω_{Im}	k_{m}	k_{c}	ω_{Im}	k_{m}	k_{c}
0.00	7.790e−04	1.387e+00	2.008e+00	–	–	–
0.50	2.759e+00	2.845e+02	5.869e+02	2.759e+00	2.845e+02	5.869e+02
0.75	1.007e+01	6.670e+02	1.666e+03	1.007e+01	6.670e+02	1.666e+03
1.00	3.033e+01	1.432e+03	3.799e+03	3.033e+01	1.432e+03	3.799e+03
1.10	2.673e+01	1.621e+03	3.871e+03	2.673e+01	1.621e+03	3.871e+03
1.50	1.161e+01	1.297e+03	2.998e+03	1.161e+01	1.297e+03	2.998e+03
2.00	6.363e+00	9.703e+02	2.314e+03	6.363e+00	9.703e+02	2.314e+03

Table 9
Table of peak values for various M (VPF: $\mu_\ell = 300$ cP, $m = 6 \times 10^{-5}$)

M	$n = 0$			$n = 1$		
	ω_{Im}	k_{m}	k_{c}	ω_{Im}	k_{m}	k_{c}
0.00	3.711e−04	9.325e−01	2.008e+00	–	–	–
0.50	1.457e−01	4.123e+01	4.492e+02	1.453e−01	4.186e+01	4.492e+02
0.75	3.735e−01	7.651e+01	1.072e+03	3.731e−01	7.723e+01	1.072e+03
1.00	1.515e+00	1.657e+02	1.531e+03	1.515e+00	1.657e+02	1.531e+03
1.10	3.803e−01	2.458e+01	1.603e+02	3.897e−01	2.413e+01	1.603e+02
1.50	1.497e−01	1.495e+01	6.733e+01	1.501e−01	1.477e+01	6.733e+01
2.00	8.965e−02	1.117e+01	4.492e+01	8.934e−02	1.090e+01	4.483e+01

where

$$\theta = \omega - kM_{\mathrm{a}}, \qquad \theta_\ell = \omega - kM_\ell. \tag{6.13}$$

Therefore the dispersion relation is expressed as

$$\left[\ell\theta^2 - \frac{2\mathrm{i}m}{R}(\kappa^2 - k^2)\theta\right]\frac{k}{\kappa}\alpha_{\mathrm{a}n} + \theta_\ell^2\alpha_n + \frac{2\mathrm{i}mk\kappa}{R}\theta\beta_{\mathrm{a}n} + \frac{2\mathrm{i}k^2}{R}\theta_\ell\beta_{ln} = W(k^2 + 4n^2 - 4)k, \tag{6.14}$$

Table 10
Table of peak values for various M (VPF: $\mu_\ell = 8000$ cP, $m = 2.25 \times 10^{-6}$)

M	$n=0$			$n=1$		
	ω_{Im}	k_{m}	k_{c}	ω_{Im}	k_{m}	k_{c}
0.00	2.656e−05	2.431e−01	2.008e+00	–	–	–
0.50	6.081e−03	1.153e+01	4.492e+02	5.959e−03	1.666e+01	4.492e+02
0.75	1.507e−02	2.260e+01	1.072e+03	1.494e−02	2.989e+01	1.072e+03
1.00	1.096e−01	5.113e+01	1.522e+03	1.095e−01	5.338e+01	1.522e+03
1.10	1.485e−02	3.511e+00	9.685e+01	2.818e−02	3.268e+00	9.712e+01
1.50	4.978e−03	2.251e+00	3.223e+01	2.056e−02	1.270e+00	2.989e+01
2.00	2.301e−03	1.801e+00	2.080e+01	1.604e−02	8.641e−01	1.927e+01

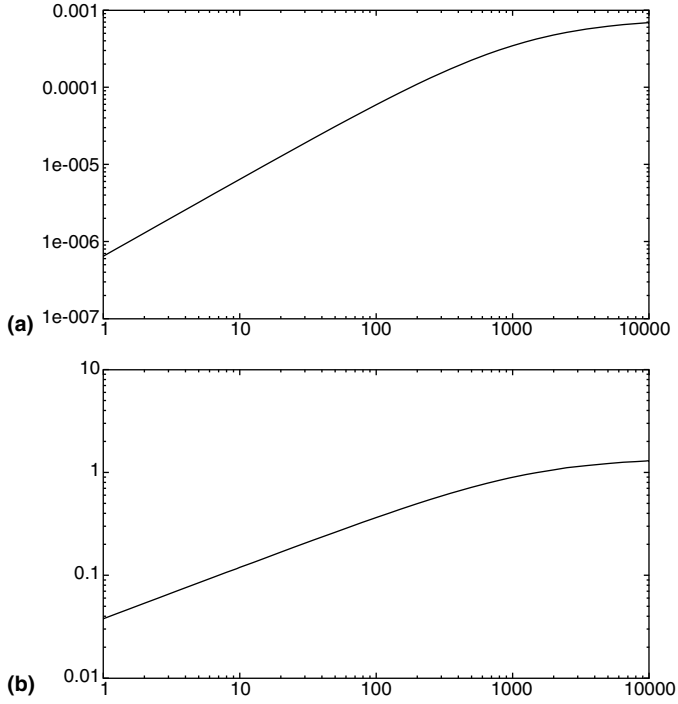

Fig. 8. (a) The maximum growth rate ω_{Im} versus R and (b) k_{m} versus R, for $M = 0$ and $n = 0$ in compressible gas. It is noted for $M = 0$ that the capillary instability may arise only for $n = 0$, but K–H instability does not arise yet.

with

$$\alpha_{\ell n} = \frac{I_n(k/2)}{I'_n(k/2)}, \quad \alpha_{an} = -\frac{K_n(\kappa/2)}{K'_n(\kappa/2)}, \quad \beta_{\ell n} = \frac{I''_n(k/2)}{I'_n(k/2)}, \quad \beta_{an} = -\frac{K''_n(\kappa/2)}{K'_n(\kappa/2)}, \tag{6.15}$$

and $\ell = \ell_0 Q(M_a)^{-1/(\gamma-1)}$, $R = R_0/Q(M_a)$, $W = W_0 Q(M_a)$ defined under (6.5).

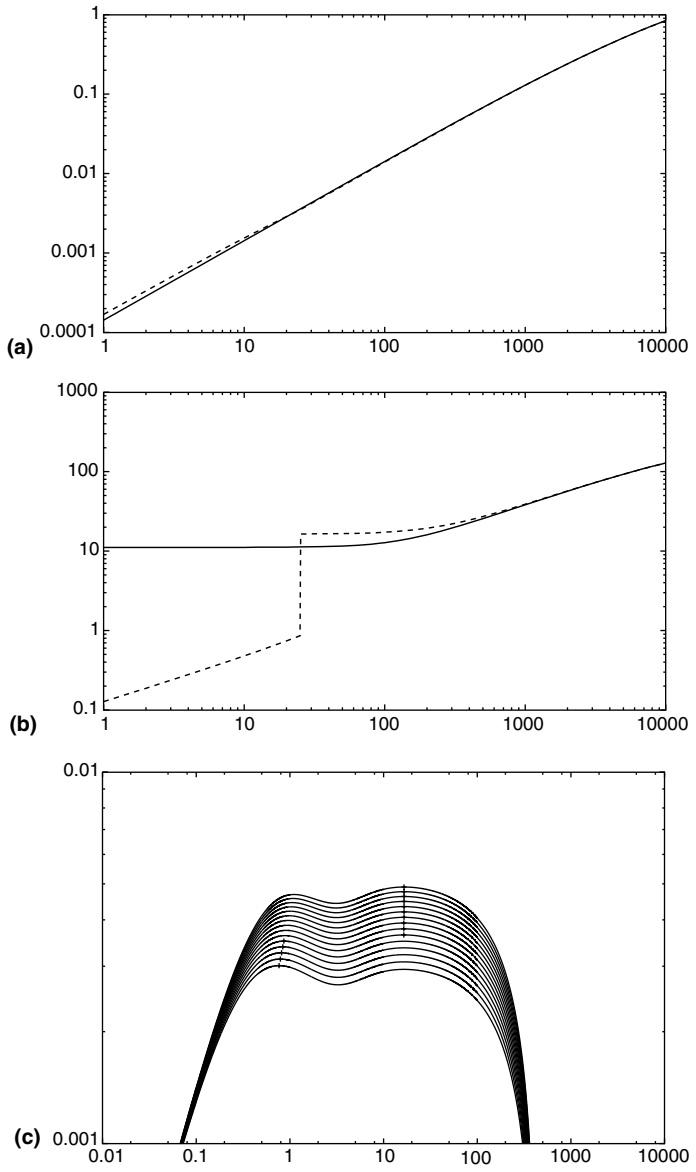

Fig. 9. (a) The maximum growth rate ω_{Im} versus R, (b) k_{m} versus R, for $M = 0.5$; $n = 0$ in compressible gas (solid line) and $n = 1$ in compressible gas (dashed line), (c) the growth rate curve ω_{I} versus k which is shown here has two relative maxima; the absolute maxima changes for R_0 between 25 and 26; this is seen as a jump in k in (b).

It is sometimes convenient to change the frame of the analysis to one moving with the liquid velocity U_ℓ. In this frame the undisturbed liquid jet is at rest and the gas moves with velocity $U_A = U_a - U_\ell$. This is a Galilean change of frame in which the new coordinates are

$$z' = z + U_\ell t \tag{6.16}$$

and

$$E = \exp(\mathrm{i}kz + \mathrm{i}n\theta - \mathrm{i}\omega_R t + \omega_I t) = \exp(\mathrm{i}kz' + \mathrm{i}n\theta - \mathrm{i}\Omega_R t + \omega_I t), \tag{6.17}$$

where

$$\Omega_R = \omega_R + U_\ell k \tag{6.18}$$

in a new frequency. However, the density, pressure and sound speed of the gas are determined by the ambient conditions and gas velocity, as in (4.3), and these quantities do not change in a Galilean change of frame. For this reason, problems of stability of liquid jets in which U_a and U_ℓ are given, as in the experiments of Varga et al. (2003) discussed in Section 12, are not simplified by a Galilean change of frame. In the analysis given in Sections 7–11 we put $M_\ell = 0$ and $M_a = M$. This is the case of a static liquid cylinder in a moving gas.

In nearly all the computations to follow, ℓ_0, R_0 and W_0 are evaluated under standard conditions for air–water given in Table 1. In Section 11 we allow W_0 to vary; this can be thought to be the effect of changing surface tension.

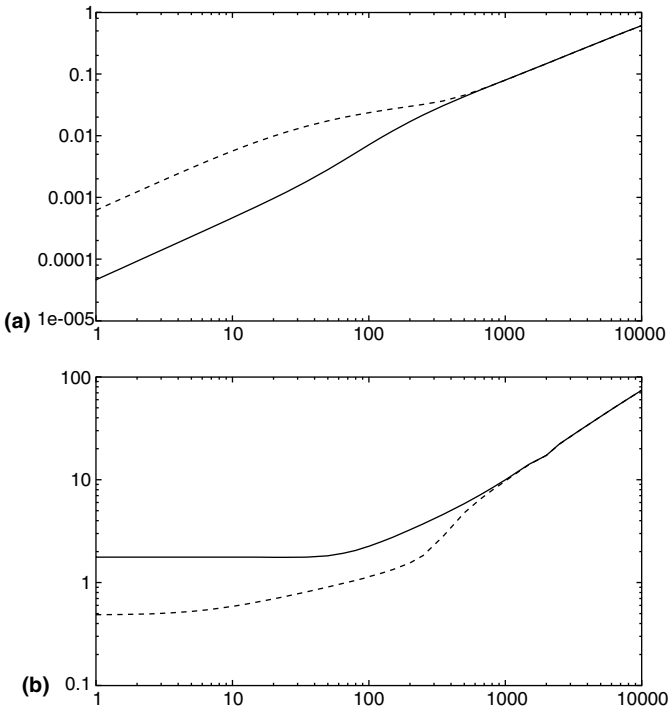

Fig. 10. (a) The maximum growth rate ω_{Im} versus R and (b) k_m versus R, for $M = 2$; $n = 0$ in compressible gas (solid line) and $n = 1$ in compressible gas (dashed line).

7. Inviscid potential flow (IPF)

The problem of an inviscid liquid jet moving in an inviscid compressible gas was considered by Li and Kelly (1992). The dispersion relation for this problem is (6.14) with $R \to \infty$ and $m/R = 0$,

$$\kappa = \sqrt{k^2 - (\omega - kM)^2}, \quad \ell(\omega - kM)^2 \frac{k}{\kappa}\alpha_{an} + \omega^2 \alpha_{\ell n} = W(k^2 + 4n^2 - 4)k. \tag{7.1}$$

The parameters of this problem are ℓ, n, M and W.

Pure capillary instability arises in the axisymmetric $n = 0$ mode for large W and in the inviscid case is independent of the gas. The case $W = 0$ is associated with pure Kelvin–Helmholtz instability for every n mode and it cannot occur in a vacuum ($\ell \neq 0$). The variation of ω_I versus k for an inviscid water in air is given in Fig. 2 with the $n = 0$ mode.

The variation of growth rates with M for particular values of k, σ, U_a was given by Li and Kelly (1992); they did not present graphs of peak growth rates ω_{Im} and k_m as a function of M. At very high values of the Mach number

$$\ell = \ell_0/Q^{2.5} \to \ell_0/M^5 \tag{7.2}$$

and the first term of (7.1) may be neglected. Growth rate curves for IPF under standard condition and different Mach numbers are shown in Fig. 2.

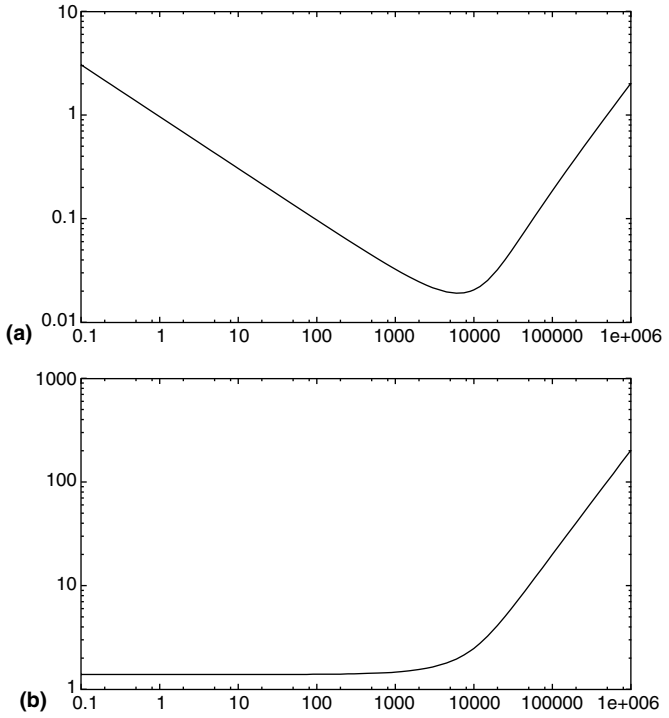

Fig. 11. (a) The maximum growth rate ω_{Im} versus W^{-1} and (b) k_m versus W^{-1}; IPF, $M = 0.5$ for $n = 0$ in compressible gas.

8. Data for liquid jets with different viscosities in an air stream

In this section the data for stability computations is assembled in Tables 2–6. In Table 2, we list the parameters for air under standard conditions and the liquid density, surface tension coefficient and the jet radius used in all the computations.

Tables 3–6 list the data used in the stability computations and the results of these computations. Each table gives results for one of four viscosities: 1, 300, 800 and 8000 cP. For each viscosity, computations were made for 27 values of U_a (Table 2) and the results of 10 cases are shown in Tables 3–6. Given μ_ℓ, U_a and the data in Table 2 the values of the material and dimensionless parameters are determined and listed in the columns of Tables 3–6. Maximum value ω_{Im} of the growth rate, the wave number k_m for $\omega_{Im} = \omega_I(k_m)$ and the wave number k_c for which $\omega_I(k_c) = 0$ (see Fig. 1. for a graphical representation of these values). Given (U_a, μ_ℓ) one may find values of M, ℓ, W and R for a dimensionless representation.

Using the parameters of Table 1, the viscosity ratio is evaluated as $m = 1.8 \times 10^{-2}$ and the other basic non-dimensional parameters which depends on U_a are shown in Table 2. Negative values $\omega_I < 0$ arise for non-axisymmetric $n = 1$ disturbances when U_a is small. The entries in the columns $n = 1$ in tables are left blanks.

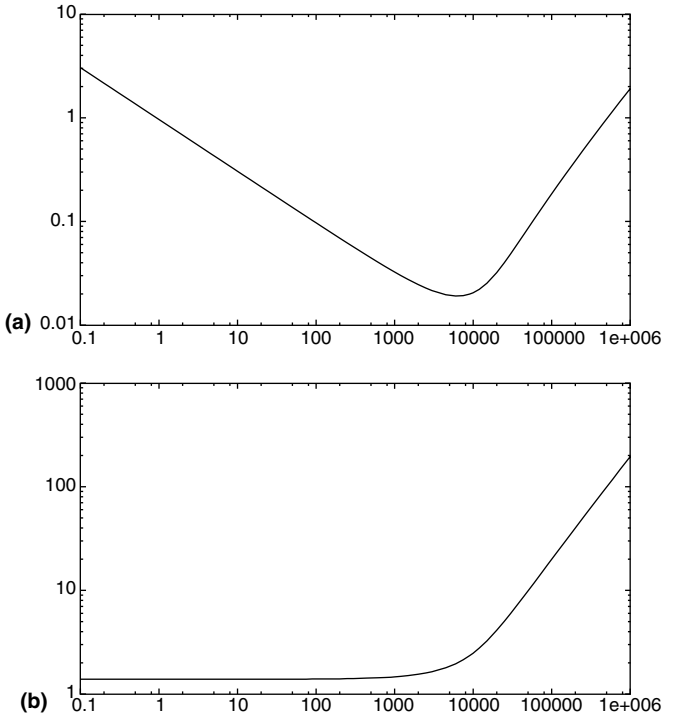

Fig. 12. (a) The maximum growth rate ω_{Im} versus W^{-1} and (b) k_m versus W^{-1}, VPF, $M = 0.5$ for $\mu_\ell = 1$ cP, for $n = 0$ in compressible gas.

9. Variation of the maximum growth rate parameters with M for different values of liquid viscosity

The variation of ω_{Im} and k_{m} with M are displayed for $\mu_\ell = 0$, 1 and 300 cP in Figs. 3–5. Results for $\mu_\ell = 8000$ cP are displayed in Fig. 6; this is a low R case for which the mode with $n = 1$ can be most dangerous. Otherwise ω_{Im} and k_{m} for the modes with $n = 0$ and $n = 1$ are essentially the same.

In Fig. 7 we blow up the sharply peaking growth rate curves ω_{I} versus k for stationary liquid jets of small viscosity in high speed transonic air. The Mach numbers for the seven curves are $[1,2,3,4,5,6,7] = [0.92, 0.96, 0.98, 1.01, 1.05, 1.08, 1.25]$ when $\mu_\ell = 0.15$ cP and $\mu_\ell = 0.175$ cP and for the nine curves $[1,2,3,4,5,6,7,8,9] = [0.92, 0.96, 1.00, 1.05, 1.06, 1.12, 1.15, 1.20, 1.25]$ when $\mu_l = 0.5$ cP. (Tables 7–10).

10. Azimuthal periodicity of the most dangerous disturbance

Batchelor and Gill (1962) argued that the conditions at the origin of a cylinder are such as to make the axisymmetric ($n = 0$) mode and the $n = 1$ mode of azimuthal periodicity most dangerous; all the modes except $n = 1$ require that the radial and azimuthal components of the

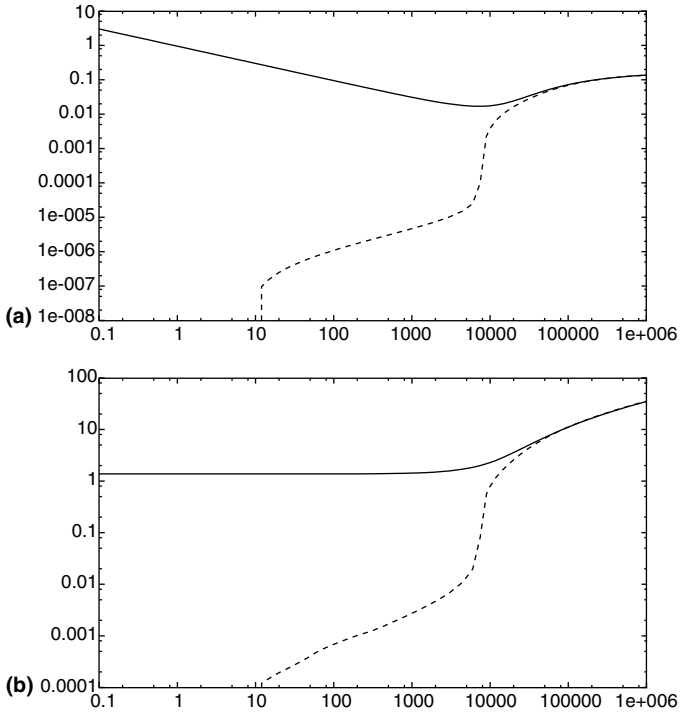

Fig. 13. (a) The maximum growth rate ω_{Im} versus W^{-1} and (b) k_{m} versus W^{-1}. VPF, $M = 0.5$ for $\mu_\ell = 300$ cP; $n = 0$ in compressible gas (solid line) and $n = 1$ in compressible gas (dashed line).

disturbance velocity vanish. The axial component of the disturbance velocity is single-valued only when $n = 0$ (see Joseph (1976, pp. 73, 74)). Typical graphs showing the variation of these quantities with the Reynolds number for $M = 0$, $M = 0.5$ and $M = 2$ are shown as Figs. 8–10. Only the axisymmetric ($n = 0$) mode gives rise to instability when $M = 0$ (Fig. 8). Inspection of Figs. 9 and 10 show that the most dangerous mode is $n = 1$ only for Reynolds numbers smaller than a number near 100; for larger Reynolds numbers the maximum growth rate and the most dangerous wave number are nearly the same for $n = 0$ and $n = 1$.

11. Variation of the growth rate parameters with the Weber number

Graphs of ω_{Im} and k_{m} versus W^{-1} are displayed for typical cases in Figs. 11–14. When W is large, the instability is dominated by capillarity; when W is small Kelvin–Helmholtz instability dominates. This behavior is characteristic also for the liquid jet in an incompressible gas which was studied by Funada et al. (2004); they used W^{-1} rather than W following earlier literature.

We have shown in Section 9 that the most dangerous mode is typically axisymmetric when the Reynolds number is larger than about 100 as is true for the cases considered here. The graphs are all similar; for small values of W^{-1} in which capillarity dominates the values of log ω_{Im} decrease linearly with log W^{-1} giving rise to a power law $\omega_{\mathrm{Im}} = a(W^{-1})^p$ where a and p may be determined

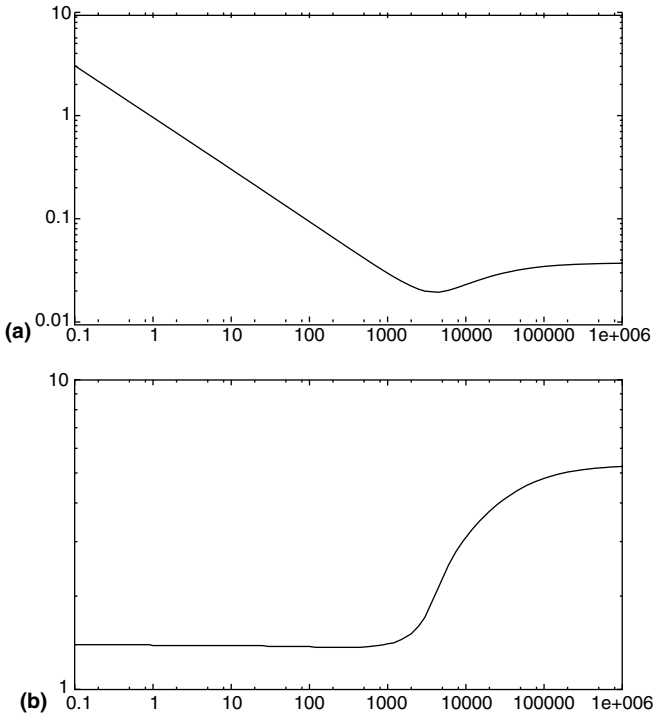

Fig. 14. (a) The maximum growth rate ω_{Im} versus W^{-1} and (b) k_{m} versus W^{-1}, VPF, $M = 2$ for $\mu_\ell = 800$ cP, for $n = 0$ in compressible gas.

from the graphs. The most dangerous wave number $k_m = 1.396$ is a universal value which maximizes ω_I when surface tension dominates. All the growth rate curves have a minimum value which marks the place where Kelvin–Helmholtz instability starts to be important, after this minimum ω_{Im} and k_m increase with W^{-1}. In all case $k_m \to \infty$ as $W^{-1} \to \infty$, but ω_{Im} is lowered as $W^{-1} \to \infty$ when the liquid viscosity is not zero (Tables 11–14).

Table 11
IPF, $M = 0.5$

W^{-1}	$n = 0$			$n = 1$		
	ω_{Im}	k_m	k_c	ω_{Im}	k_m	k_c
1.00e−01	3.071e+00	1.396e+00	–	–	–	–
1.00e+00	9.710e−01	1.396e+00	–	–	–	–
1.00e+01	3.072e−01	1.396e+00	–	–	–	–
1.00e+02	9.770e−02	1.405e+00	–	–	–	–
1.00e+03	3.272e−02	1.468e+00	–	–	–	–
1.00e+04	2.062e−02	2.485e+00	–	4.306e−03	8.614e−01	–
1.00e+05	1.865e−01	2.008e+01	2.656e+01	1.833e−01	1.990e+01	2.539e+01
1.00e+06	2.037e+00	2.035e+02	–	2.037e+00	2.035e+02	2.710e+02

Table 12
VPF, $M = 0.5$ for $\mu_\ell = 1$ cP

W^{-1}	$n = 0$			$n = 1$		
	ω_{Im}	k_m	k_c	ω_{Im}	k_m	k_c
1.00e−01	3.071e+00	1.396e+00	1.999e+00	–	–	–
1.00e+00	9.710e−01	1.396e+00	1.999e+00	–	–	–
1.00e+01	3.072e−01	1.396e+00	1.999e+00	5.123e−08	3.862e−04	1.495e−01
1.00e+02	9.769e−02	1.405e+00	2.026e+00	1.109e−06	2.251e−03	6.967e−01
1.00e+03	3.272e−02	1.468e+00	2.287e+00	4.767e−06	9.766e−03	1.504e+00
1.00e+04	2.061e−02	2.485e+00	5.338e+00	4.304e−03	8.605e−01	4.618e+00
1.00e+05	1.854e−01	1.999e+01	4.024e+01	1.822e−01	1.990e+01	4.015e+01
1.00e+06	1.921e+00	1.963e+02	3.988e+02	1.921e+00	1.963e+02	3.988e+02

Table 13
VPF, $M = 0.5$ for $\mu_\ell = 300$ cP

W^{-1}	$n = 0$			$n = 1$		
	ω_{Im}	k_m	k_c	ω_{Im}	k_m	k_c
1.00e−01	3.070e+00	1.396e+00	1.999e+00	–	–	–
1.00e+00	9.701e−01	1.396e+00	1.999e+00	–	–	–
1.00e+01	3.063e−01	1.396e+00	1.999e+00	–	–	8.686e−03
1.00e+02	9.677e−02	1.396e+00	2.008e+00	1.108e−06	6.931e−04	4.033e−02
1.00e+03	3.172e−02	1.450e+00	2.107e+00	4.758e−06	2.755e−03	8.326e−02
1.00e+04	1.784e−02	2.314e+00	3.502e+00	3.862e−03	8.011e−01	1.288e+00
1.00e+05	7.341e−02	1.126e+01	2.962e+01	7.055e−02	1.126e+01	2.944e+01
1.00e+06	1.396e−01	3.538e+01	3.052e+02	1.391e−01	3.583e+01	3.052e+02

Table 14
VPF, $M = 2$ for $\mu_\ell = 800$ cP

W^{-1}	$n = 0$			$n = 1$		
	ω_{Im}	k_m	k_c	ω_{Im}	k_m	k_c
1.00e−01	3.068e+00	1.396e+00	1.999e+00	–	–	–
1.00e+00	9.679e−01	1.387e+00	1.999e+00	–	–	9.964e−03
1.00e+01	3.040e−01	1.387e+00	1.999e+00	–	–	2.890e−02
1.00e+02	9.455e−02	1.378e+00	2.017e+00	–	–	5.959e−02
1.00e+03	2.992e−02	1.405e+00	2.224e+00	–	–	–
1.00e+04	2.312e−02	3.097e+00	5.203e+00	3.096e−02	1.819e+00	4.078e+00
1.00e+05	3.464e−02	4.807e+00	1.207e+01	3.919e−02	3.367e+00	1.189e+01
1.00e+06	3.728e−02	5.257e+00	2.935e+01	4.094e−02	3.844e+00	2.926e+01

12. Coaxial jets

The problem of a liquid jet in a compressible gas flow is encountered in atomization experiments in coaxial jets discussed by Varga et al. (2003). They observed that the jet undulates due to Kelvin–Helmholtz instability and in the undulated configuration is at an angle to the air. The air stream then has a component normal to the KH waves giving rise to a secondary Rayleigh–Taylor instability which they claim is the primary cause of breakup. The analysis of this secondary instability is beyond the scope of our linear theory.

Varga et al. (2003) gave experimental results for jets of water and ethanol of different diameter and various jet speeds U_ℓ and air speeds ranging flow 40–165 m/s. The air speeds are subsonic and even at the highest air speed (165 m/s) the effects of compressibility are modest. We carried out calculations for some of their experiments with data summarized in Table 15. The growth rate curves in all these cases are like that shown in Fig. 1 so that it will suffice to present the results in the forms of tables of maximum growth rate parameters. In all cases, the growth rates are larger for the axisymmetric mode $n = 0$ than for the mode with $n = 1$. However the maximum growth rates for $n = 1$ are not much smaller so that mixture of these modes might be expected to occur in experiments. Mixed modes are existent in the experiments of Varga et al. (2003).

In Figs. 15 and 16 we present graphs of ω_{Im}, k_m and k_c versus U_ℓ for coaxial jets of liquid into air studied by Varga et al. (2003) when $U_a = 40$ m/s under conditions listed in Tables 16. In Fig. 17 the same data is given for $U_a = 165$ m/s and in Fig. 18 for $U_a = 265$ m/s (Tables 17–19).

Table 15
(Varga et al., 2003) Fluid properties

Fluid	Density (kg m^{-3})	Viscosity (Pa s)	Surface tension (N/m)
Air	1.2	1.8×10^{-5}	–
Water	998	1.0×10^{-3}	0.070
Ethanol	791	1.2×10^{-3}	0.023

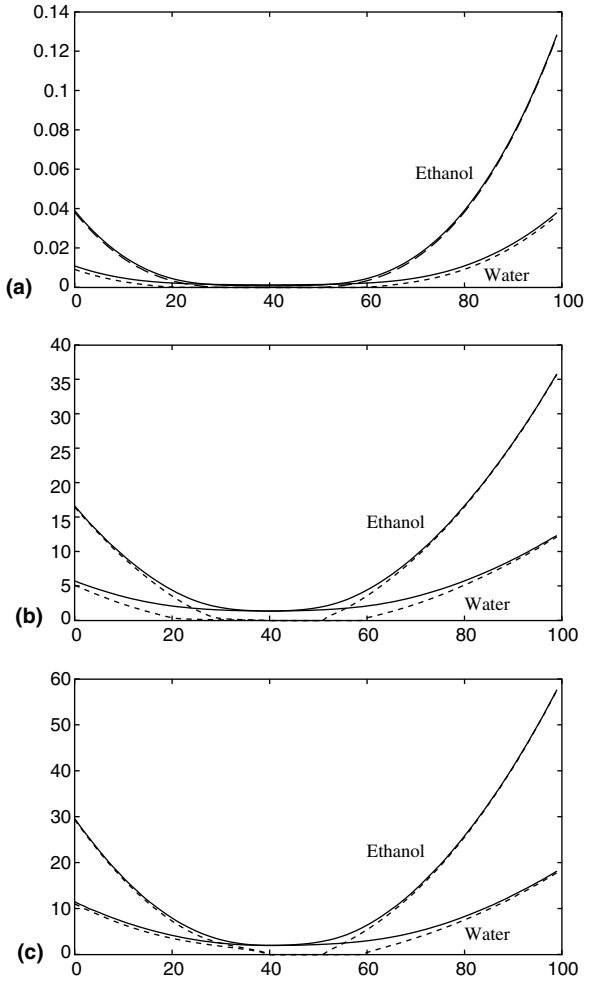

Fig. 15. KH instability of liquid jet with U_ℓ in compressible gas of $U_a = 40$ m/s for $0 < U_\ell < 100$ m/s. $n = 0$ solid lines, $n = 1$ dashed lines. (a) The maximum growth rate ω_{Im} versus U_ℓ, (b) the maximum growth wave number k_m versus U_ℓ and (c) the cut-off wave number k_c versus U_ℓ.

13. Convective/absolute (C/A) instability

C/A instability is used to determine when the spatial theory of instability makes sense. Practically, this comes down to a determination of the conditions under which a disturbance from a localized source will propagate downstream without corrupting the source. The disturbance may grow as it propagates but after it passes over a fixed point it leaves the flow undisturbed. This is the case for convectively unstable flows, but absolutely unstable flows propagate both upstream and downstream. Propagation of disturbances from a vibrating ribbon in a boundary layer or Poiseuille flow are examples. For such propagation these flows must be convectively and not absolutely unstable.

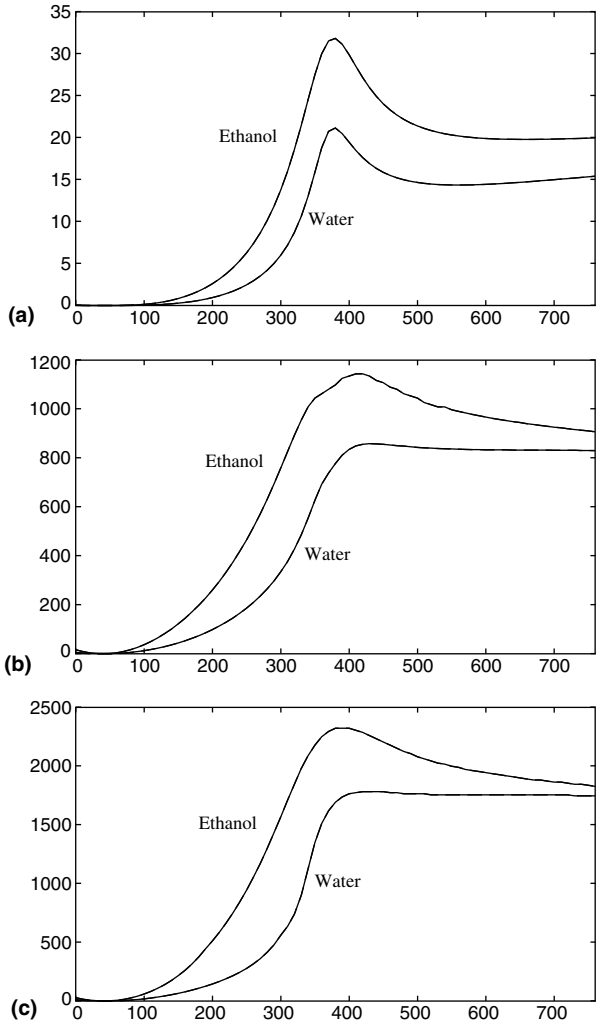

Fig. 16. KH instability of liquid jet with U_ℓ in compressible gas of $U_a = 40$ m/s for $0 < U_\ell < 800$ m/s. $n = 0$ solid lines. The graphs for $n = 1$ coincide with $n = 0$ for large values of U_ℓ. (a) The maximum growth rate ω_{Im} versus U_ℓ, (b) the maximum growth wave number k_m versus U_ℓ and (c) the cut-off wave number k_c versus U_ℓ.

The study of stability of disturbances issuing from a fixed source, leading to C/A theory, is not a complete stability theory; the traditional temporal theory of instability needs also to be considered. The temporal theory determines the conditions under which disturbances at a fixed point will grow or decay. If these conditions are such that all disturbances decay, then disturbances from a fixed point will decay. Disturbances which are convectively or absolutely unstable are also temporally unstable. The propagation of impulses from a source in a convectively unstable flow can be realized provided the growth rates and amplitudes of temporally unstable flows do not corrupt the flow first. This is why experiments with vibrating ribbons are always done with care to suppress background noise which may amplify in time a fixed point.

Table 16
ω_{Im}, k_m and k_c for $U_a = 40$ m/s $U_\ell = 60$, 160, 260, 360, 460, 560, 660, 760 m/s. (1) water $n = 0$, (2) water $n = 1$, (3) ethanol $n = 0$ and (4) ethanol $n = 1$

		Compressible gas		
	U_ℓ	ω_{Im}	k_m	k_c
(1)	60	2.067e−01	3.601e+01	6.904e+01
	160	1.396e−03	1.423e+00	2.116e+00
	260	1.500e−01	2.926e+01	4.321e+01
	360	1.647e+00	1.414e+02	2.053e+02
	460	1.106e+01	4.888e+02	1.018e+03
	560	1.347e+01	7.597e+02	1.585e+03
	660	1.200e+01	7.444e+02	1.567e+03
	760	1.226e+01	7.408e+02	1.567e+03
(2)	60	2.057e−01	3.601e+01	6.895e+01
	160	9.133e−06	6.310e−02	1.144e+00
	260	1.489e−01	2.917e+01	4.312e+01
	360	1.647e+00	1.414e+02	2.053e+02
	460	1.106e+01	4.888e+02	1.018e+03
	560	1.347e+01	7.597e+02	1.585e+03
	660	1.200e+01	7.444e+02	1.567e+03
	760	1.226e+01	7.408e+02	1.567e+03
(3)	60	6.305e−01	1.009e+02	1.900e+02
	160	9.394e−04	1.477e+00	2.260e+00
	260	4.663e−01	8.236e+01	1.387e+02
	360	4.354e+00	3.610e+02	7.201e+02
	460	2.093e+01	8.866e+02	1.810e+03
	560	2.076e+01	9.910e+02	1.954e+03
	660	1.724e+01	8.947e+02	1.783e+03
	760	1.674e+01	8.461e+02	1.693e+03
(4)	60	6.302e−01	1.009e+02	1.900e+02
	160	2.000e−05	1.252e−01	1.387e+00
	260	4.658e−01	8.236e+01	1.387e+02
	360	4.353e+00	3.610e+02	7.201e+02
	460	2.092e+01	8.866e+02	1.810e+03
	560	2.076e+01	9.910e+02	1.954e+03
	660	1.724e+01	8.947e+02	1.783e+03
	760	1.674e+01	8.461e+02	1.693e+03

Li and Kelly (1992) considered the convective and absolute instability of an inviscid liquid jet in an air stream of an inviscid compressible gas. They motivated their study by experiments on the instability and breakup of liquid fuel jets in crossflow. They note that

> "... the breakup of the jet, however, does not seem to proceed in the gradual manner typical of the capillary instability of a liquid jet issuing into air at rest. Here the jet gradually bends over toward the direction of the free stream so that both tangential and crossflow components of the gas flow are seen by the jet. When the jet is at an angle of about 30° from the normal to the free stream, the jet breaks into large columns in a manner so sudden that

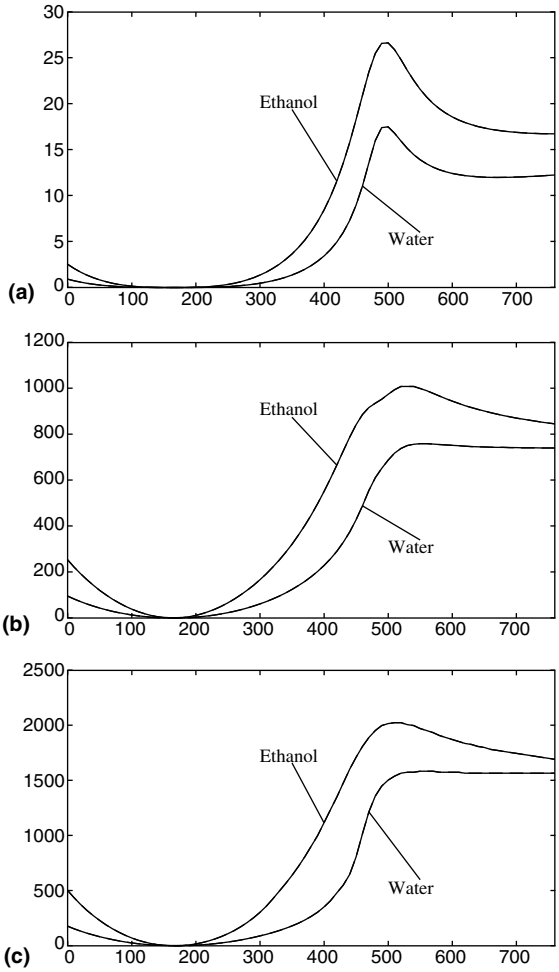

Fig. 17. KH instability of liquid jet with U_ℓ in compressible gas of $U_a = 165$ m/s and $0 < U_\ell < 800$ m/s. $n = 0$ solid lines, $n = 1$ dashed lines. The solid line ($n = 0$) overlaps with the dashed line ($n = 1$). (a) The maximum growth rate ω_{Im} versus U_ℓ, (b) the maximum growth wave number k_m versus U_ℓ and (c) the cut-off wave number k_c versus U_ℓ.

> Schetz and co-workers (Sherman and Schetz, 1971; Schetz et al., 1980) have used the phrase "fracture" to describe the phenomenon. At this angle, the component of the gas velocity parallel to the jet's direction is approximately sonic ..."

Li and Kelly (1992) did not study a jet in crossflow; they studied a liquid in a coflowing air stream. They also considered the convective and absolute instability of a plane jet and found transition to absolute instability in the transonic region. They speculate that fracture coincides with the transition to absolute instability.

The problem considered by Li and Kelly (1992), C/A instability of a plane jet, is rather far from experiments on crossflow of Sherman and Schetz (1971) and it could be considered in the frame of temporal combined Rayleigh–Taylor, Kelvin–Helmholtz instability which should show rather

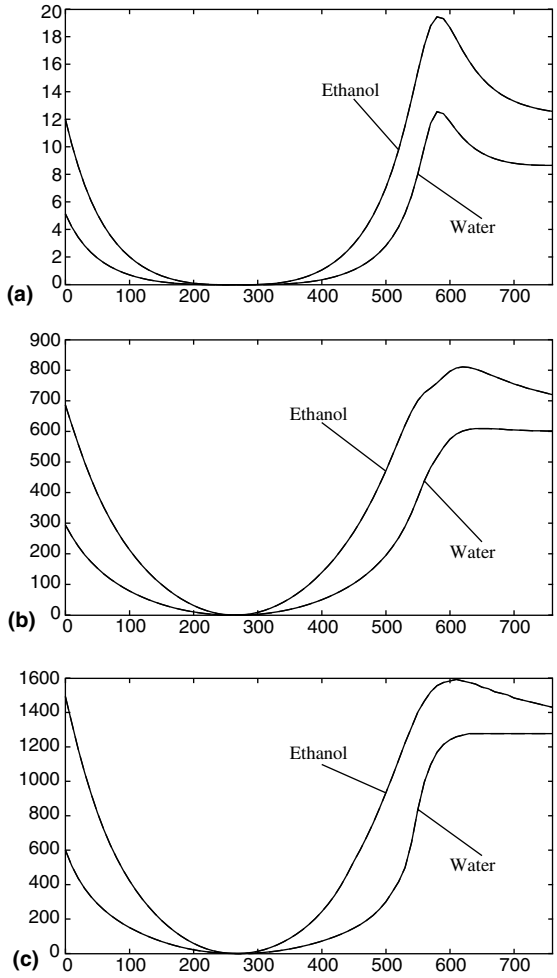

Fig. 18. KH instability of liquid jet with U_ℓ in compressible gas of $U_a = 265$ m/s. $n = 0$ solid lines, $n = 1$ dashed lines. The solid line ($n = 0$) overlaps with the dashed line ($n = 1$). (a) The maximum growth rate ω_{Im} versus U_ℓ, (b) the maximum growth wave number k_m versus U_ℓ and (c) the cut-off wave number k_c versus U_ℓ.

Table 17
Parameters for $U_a = 40$ m/s

Fluid	U_a (m/s)	D_ℓ (m)	M_a	W_e	R_e	m	ℓ
Water	4.000e+01	3.200e−04	1.178e−01	1.901e−06	1.084e+05	1.800e−02	1.194e−03
Ethanol	4.000e+01	3.200e−04	1.178e−01	7.882e−0.7	7.162e+04	1.500e−02	1.507e−03

exceptional behavior in transonic flow. This kind of explanation of rapid breakup of a coflowing jet was given by Varga et al. (2003) and it is based on a secondary RT instability not associated with absolute instability.

Table 18
Parameters for $U_a = 165$ m/s

Fluid	U_a (m/s)	D_ℓ (m)	M_a	W_e	R_e	m	ℓ
Water	1.650e+02	3.200e−04	4.971e−01	1.990e−06	1.060e+05	1.800e−02	1.066e−03
Ethanol	1.650e+02	3.200e−04	4.971e−01	8.249e−07	7.001e+04	1.500e−02	1.345e−03

Table 19
Parameters for $U_a = 265$ m/s

Fluid	U_a (m/s)	D_ℓ (m)	M_a	W_e	R_e	m	ℓ
Water	2.650e+02	3.200e−04	8.316e−01	2.158e−06	1.018e+05	1.800e−02	8.698e−04
Ethanol	2.650e+02	3.200e−04	8.316e−01	8.947e−07	6.722e+04	1.500e−02	1.097e−03

14. Conclusions

We studied the temporal instability of a liquid jet in a high speed compressible air stream using viscous potential flow. Since the shear stress is ignored in viscous potential flow, the analysis is compatible with the discontinuous profile used in all studies of Kelvin–Helmholtz instability. This discontinuity is not allowable for real viscous fluids where shear layers develop. Disturbances with high wave numbers might see the details of the shear layer and alter the stability results in ways which are presently unknown.

In our analysis, which neglect shear layers, this instability is dominated by capillarity when the Weber number is large and by Kelvin–Helmholtz instability when the Weber number is small. The peak growth rates and the associated wavelengths depend strongly on the Mach number and on the viscosity of the liquid. The growth rates are dramatically larger in the transonic region and the wavelengths of the peak values are much smaller. Viscosity reduces the magnitude of the growth. The growth rate for inviscid potential flow monotonically increases as Mach number increases. For $0 < \mu_\ell < 0.168$ cP, the growth rate for viscous potential flow monotonically increases as Mach number increases. For 0.168 cP $< \mu_\ell$, the growth rate for viscous potential flow has a peak value when Mach number is nearly one. The peak value decreases as the viscosity μ_ℓ increases. The growth rates are very sharply peaked near $M_a = 1$ when the viscosity is larger than some value near 0.2 cP. The dramatic change in stability of liquid jets in transonic flow predicted by analysis is possibly related to the dramatic increases in the drag coefficient of spheres and disks in transonic flow observed in experiments (Howarth (1953, p. 724)). It is not known if jet breakup in transonic and supersonic flow is caused directly by KH instability or through a secondary RT instability. In either case, this analysis suggests that the drop fragments would be very small.

Acknowledgement

This work was supported by the NSF/CTS-0076648, the Engineering Research Program of the Office of Basic Energy Sciences at the DOE.

References

Batchelor, G.K., Gill, A.E., 1962. Analysis of the stability of axisymmetric jets. J. Fluid Mech. 14, 529–551.
Chang, I.-D., Russel, P.E., 1965. Stability of a liquid layer adjacent to a high-speed gas stream. Phys. Fluids 8, 1018–1026.
Chawla, T.C., 1975. The Kelvin–Helmholtz instability of the gas–liquid interface of a sonic gas jet submerged in a liquid. J. Fluid Mech. 67, 513–537.
Chen, T., Li, X., 1999. Liquid jet atomization in a compressible gas stream. J. Propul. Power 15, 369–376.
Dunne, B., Cassen, B., 1954. Some phenomena associated with supersonic liquid jets. J. Appl. Phys. 25, 569–572.
Dunne, B., Cassen, B., 1956. Velocity discontinuity instability of a liquid jet. J. Appl. Phys. 27, 577–582.
Engel, O.G., 1958. Fragmentation of waterdrops in the zone behind an air shock. J. Res. Natl. Bur. Stand. 60, 245–280.
Funada, T., Joseph, D.D., 2001. Viscous potential flow analysis of Kelvin–Helmholtz instability in a channel. J. Fluid Mech. 445, 263–283.
Funada, T., Joseph, D.D., 2002. Viscous potential flow analysis of capillary instability. Int. J. Multiphase Flow 28, 1459–1478.
Funada, T., Joseph, D.D., Yamashita, S., 2004. Stability of a liquid jet into incompressible gases and liquids. Int. J. Multiphase Flow 30, 1279–1310.
Howarth, L., 1953. Modern Developments in Fluid Dynamics: High Speed Flow. Clarendon Press, Oxford.
Joseph, D.D., 2003. Viscous potential flow. J. Fluid Mech. 479, 191–197.
Joseph, D.D., Belanger, J., Beavers, G.S., 1999. Breakup of a liquid drop suddenly exposed to a high-speed airstream. Int. J. Multiphase Flow 25, 1263–1303.
Joseph, D.D., Beavers, G.S., Funada, T., 2002. Rayleigh–Taylor instability of viscoelastic drops at high Weber numbers. J. Fluid Mech. 453, 109–132.
Joseph, D.D., 1976. Stability of Fluid Motions, I and II, Springer Tracts in Natural Philosophy, vols. 27 and 28. Springer-Verlag, Berlin–Heidelberg–New York.
Li, H.-S., Kelly, R.E., 1992. The instability of a liquid jet in a compressible airstream. Phys. Fluids A4, 2162–2168.
Lin, S.P., 2003. Breakup of Liquid Sheets and Jets. Cambridge University Press.
Nayfeh, A.H., Saric, W.S., 1973. Nonlinear stability of a liquid film adjacent to a supersonic stream. J. Fluid Mech. 58, 39–51.
Schetz, J.A., Kush, E.A., Joshi, P.B., 1980. Wave phenomena in liquid jet breakup in a supersonic crossflow. AIAA J. 18, 774–778.
Sherman, A., Schetz, J.A., 1971. Breakup of liquid sheets and jets in a supersonic gas stream. AIAA J. 9, 666–673.
Theofanous, T.G., Li, G.J., Dinh, T.N., 2003. Aerobreakup in rarefied supersonic gas flows. In: Proceedings of FEDSM03 4-th ASME/JSME Joint Fluids Engineering Conference.
Varga, C.M., Lasheras, J.C., Hopfinger, E.J., 2003. Initial breakup of a small-diameter liquid jet by a high-speed gas stream. J. Fluid Mech. 497, 405–434.
Zhou, Z.W., Lin, S.P., 1992. Absolute and convective instability of a compressible jet. Phys. Fluids A4, 277–282.